Numerical method for the equilibrium configurations of a Maier-Saupe bulk potential in a Q-tensor model of an anisotropic nematic liquid crystal

Cody D. Schimming[1]

School of Physics and Astronomy
University of Minnesota, Minneapolis, MN 55455

Jorge Viñals[2]

School of Physics and Astronomy
University of Minnesota, Minneapolis, MN 55455

Shawn W. Walker*

Department of Mathematics
Center for Computation and Technology (CCT)
Louisiana State University,
Baton Rouge, LA 70803 Tel.: +1-225-578-1603
Fax: +1-225-578-4276

Abstract

We present a numerical method, based on a tensor order parameter description of a nematic phase, that allows fully anisotropic elasticity. Our method thus extends the Landau-de Gennes **Q**-tensor theory to anisotropic phases. A microscopic model of the nematogen is introduced (the Maier-Saupe potential in the case discussed in this paper), combined with a constraint on eigenvalue bounds of **Q**. This ensures a physically valid order parameter **Q** (i.e., the eigenvalue bounds are maintained), while allowing for more general gradient energy densities that can include cubic nonlinearities, and therefore elastic anisotropy. We demonstrate the method in two specific two dimensional examples in which the Landau-de Gennes model including elastic anisotropic is known to fail, as well as in three dimensions for the cases of a hedgehog point defect, a disclination line, and a disclination ring. The details of the numerical implementation are also discussed.

Keywords: liquid crystals, defects, Landau-de Gennes, finite element method,

*Corresponding author; S. W. Walker acknowledges financial support by the NSF DMS-1555222 (CAREER).

Email addresses: schim111@umn.edu (Cody D. Schimming), walker@math.lsu.edu (Shawn W. Walker)

[1]C. D. Schimming acknowledges financial support by NSF DMR-1838977.

[2]J. Viñals acknowledges financial support by NSF DMR-1838977.

singular bulk potential
2010 MSC: 65N30, 49M25, 35J70

1. Introduction

Liquid crystals (LCs) are a critical material for emerging technologies [1, 2]. Their response to optical [3, 4, 5, 6, 7], electric/magnetic [8, 9, 10], and mechanical actuation [11, 12, 13, 14] has already yielded various devices, e.g. electronic shutters [15], novel types of lasers [16, 17], dynamic shape control of elastic bodies [18, 19], and others [20, 21, 22, 23, 24]. Furthermore, in the emerging field of active matter, self propulsion often leads to nematic order, both because of the broken symmetry in motion induced by the constituent particles, and because the elongated particles themselves promote liquid crystalline ordering [25, 26]. Fruitful connections are being found with such disparate areas of Biology as rearrangements in confluent epithelial tissue [27], neural stem cell cultures [28], or cellular motors comprising microtubule bundles and kinesin complexes [29].

LCs are a *meso-phase* of matter in which its ordered macroscopic state is *between* a spatially disordered liquid, and a fully crystalline solid [30]. In their nematic phase, in which long ranged orientational order exists, the Landau-de Gennes (LdG) theory introduces a *tensor-valued* function $\mathbf{Q}$ to describe local order in the LC material. In particular, the eigenframe of $\mathbf{Q}$ yields information about the statistics of the distribution of LC molecule orientations. The energy functional of $\mathbf{Q}$ that describes the LC material involves both a bulk potential, and an elastic contribution involving the derivatives of $\mathbf{Q}$.

Unlike the related description of a LC nematic phase in terms of a director, the analysis based on $\mathbf{Q}$ is generally limited to the so called one constant approximation, appropriate for an elastically isotropic phase. In this case, the Landau-de Gennes energy is supplemented by a gradient term of the form $L_1|\nabla\mathbf{Q}|^2$, where L_1 is the elastic constant. Inclusion of elastic anisotropy requires gradient terms at least of third order in $\mathbf{Q}$. Unfortunately, at this order, the energy is known to become unbounded for any choice of parameters [31, 32]. Therefore, in principle, the requirement of a stable energy would imply consideration of terms at least of fourth order in gradients. Since there are 22 possible fourth order invariants allowed by symmetry [33], the Landau-de Gennes theory becomes overly complex for anisotropic systems.

This paper develops an alternative method to the LdG model that uses a special type of *singular* bulk potential, the so-called Ball-Majumdar potential [31]. This potential has the following desirable properties: (i), it can be derived from a microscopic interaction potential by using the tools of statistical mechanics; and (ii), it enforces that $\mathbf{Q}$ has physically permissible eigenvalues. However, this choice of potential introduces some novel difficulties that are not present in the standard LdG model, chief among them is that in the implementation the energy as a function of $\mathbf{Q}$ does not have a closed form, rather it needs to be evaluated entirely numerically. This is analogous to other self consistent field theories as applied, for example, to polymers [34]. Many numerical

methods and implementations already exist for the standard LdG model, e.g. [35, 36, 37, 38, 39, 40, 41]. However, numerical methods for the Ball-Majumdar potential have been given only recently [42, 43]. In this paper we formalize this prior work, contrast its results with the LdG model in cases in which the latter fails, and also show the power of the method by computing defect configurations in three spatial dimensions.

2. Liquid Crystal Theory

We briefly review in this section the Landau-de Gennes theory for a nematic phase, as well as the more microscopic Maier-Saupe theory. Consider an anisotropic LC molecule which is uniaxial, with orientation described by the unit vector $\mathbf{p}$. The Maier-Saupe potential between two molecules i and j is a contact interaction of the form $-\kappa\left((\mathbf{p}_i \cdot \mathbf{p}_j)^2 - 1/3\right)$, where κ is the interaction constant [1]. In the isotropic phase, the thermal average of $\mathbf{p}$ is zero, while it is nonzero in the nematic phase. The Landau-de Gennes theory of a nematic phase is formulated instead in terms of a mesoscopic order parameter, the symmetric, traceless tensor $\mathbf{Q}$. In the isotropic phase $\mathbf{Q} = \mathbf{0}$. In the nematic phase, $\mathbf{Q}$ is nonzero. A uniaxial nematic phase corresponds to two of the eigenvalues of $\mathbf{Q}$ being equal, and a biaxial phase to the general case. Note that although the molecules themselves are uniaxial, the distribution of local orientations may itself be uniaxial or biaxial.

2.1. Landau-de Gennes Theory

Let $\mathbf{\Xi}$ be the set of symmetric, traceless 3×3 matrices. Given a tensor-valued function $\mathbf{Q} : \Omega \to \mathbf{\Xi}$, where Ω is a physical domain with Lipschitz boundary Γ, the free energy of the LdG model is defined as [44, 45]:

$$\begin{aligned} E[\mathbf{Q}] := \int_\Omega \mathcal{W}(\mathbf{Q}, \nabla\mathbf{Q})\, d\mathbf{x} + \frac{1}{\epsilon^2}\int_\Omega \psi(\mathbf{Q})\, d\mathbf{x} \\ + \eta_\Gamma \int_\Gamma f_\Gamma(\mathbf{Q})\, dS(\mathbf{x}) - \int_\Omega \chi(\mathbf{Q})\, d\mathbf{x}, \end{aligned} \tag{1}$$

with

$$\begin{aligned} \mathcal{W}(\mathbf{Q}, \nabla\mathbf{Q}) := \frac{1}{2}\Big(L_1|\nabla\mathbf{Q}|^2 + L_2|\nabla\cdot\mathbf{Q}|^2 + L_3(\nabla\mathbf{Q})^T \vdots \nabla\mathbf{Q}, \\ + L_4\nabla\mathbf{Q} \vdots (\mathbf{e}\cdot\mathbf{Q}) + L_*\nabla\mathbf{Q} \vdots [(\mathbf{Q}\cdot\nabla)\mathbf{Q}]\Big), \end{aligned} \tag{2}$$

where $\{L_i\}_{i=1}^4$, L_*, are material dependent elastic constants, and

$$\begin{aligned} |\nabla\mathbf{Q}|^2 := (\partial_k Q_{ij})^2, \quad |\nabla\cdot\mathbf{Q}|^2 := (\partial_j Q_{ij})^2, \quad (\nabla\mathbf{Q})^T \vdots \nabla\mathbf{Q} := (\partial_j Q_{ik})(\partial_k Q_{ij}), \\ \nabla\mathbf{Q} \vdots (\mathbf{e}\cdot\mathbf{Q}) := e_{jkl}Q_{ji}\partial_l Q_{ki}, \quad \nabla\mathbf{Q} \vdots [(\mathbf{Q}\cdot\nabla)\mathbf{Q}] := Q_{lk}(\partial_l Q_{ij})(\partial_k Q_{ij}). \end{aligned} \tag{3}$$

We use the convention of summation over repeated indices. Energies in Eq. (1) are made dimensionless by writing them in units of the temperature, T, while

lengths are scaled by a characteristic length ξ. The value of the dimensionless parameter $\epsilon^2 \equiv L_1/(T\xi^2)$ determines the relative weight of the gradient dependent energy $\mathcal{W}(\mathbf{Q}, \nabla\mathbf{Q})$ to the bulk potential $\psi(\mathbf{Q})$ and thus determines ξ [46]. All five elastic constants can be related to the five independent constants of the Oseen-Frank model (i.e. K_1, K_2, K_3, K_4, and the twist q_0) [44, 45]. Indeed, L_4 accounts for twist and L_* is needed to have five independent constants. Note that taking $L_i = 0$, for $i = 2, 3, 4$, and $L_* = 0$ gives the one constant LdG model. More complicated models can also be considered [45, 1, 47]. The bulk potential $\psi(\mathbf{Q})$ is discussed in the next subsection.

The surface energy $f_\Gamma(\mathbf{Q})$, with parameter $\eta_\Gamma \geq 0$, accounts for *weak anchoring* of the LC (i.e. penalization of boundary conditions). For example, a Rapini-Papoular type anchoring energy [48] can be considered:

$$f_\Gamma(\mathbf{Q}) = \frac{1}{2}\mathrm{tr}\,(\mathbf{Q} - \mathbf{Q}_\Gamma)^2 \equiv \frac{1}{2}|\mathbf{Q} - \mathbf{Q}_\Gamma|^2, \tag{4}$$

where $\mathbf{Q}_\Gamma(\mathbf{x}) \in \boldsymbol{\Xi}$ for all $\mathbf{x} \in \Gamma$.

The function $\chi(\cdot)$ accounts for interactions with external fields (e.g., an electric field). For example, the energy density of a dielectric LC with fixed boundary potential is given by $-1/2\,\mathbf{D}\cdot\mathbf{E}$ [49], where the electric displacement $\mathbf{D}$ is related to the electric field $\mathbf{E}$ by the linear constitutive law [50, 1, 51]:

$$\mathbf{D} = \boldsymbol{\varepsilon}\mathbf{E} = \bar{\varepsilon}\mathbf{E} + \varepsilon_\mathrm{a}\mathbf{Q}\mathbf{E}, \quad \boldsymbol{\varepsilon}(\mathbf{Q}) = \bar{\varepsilon}\mathbf{I} + \varepsilon_\mathrm{a}\mathbf{Q}, \tag{5}$$

where $\boldsymbol{\varepsilon}$ is the LC material's dielectric tensor and $\bar{\varepsilon}$, ε_a are constitutive dielectric permittivities. Thus, in the presence of an electric field, $\chi(\cdot)$ becomes

$$\chi(\mathbf{Q}) = -\frac{1}{2}\mathbf{D}\cdot\mathbf{E} = -\frac{1}{2}\left[\bar{\varepsilon}|\mathbf{E}|^2 + \varepsilon_\mathrm{a}\mathbf{E}\cdot\mathbf{Q}\mathbf{E}\right]. \tag{6}$$

2.2. Landau-de Gennes bulk potential

The bulk potential ψ is a double-well type of function that is given by

$$\psi(\mathbf{Q}) = K - \frac{A}{2}\mathrm{tr}(\mathbf{Q}^2) - \frac{B}{3}\mathrm{tr}(\mathbf{Q}^3) + \frac{C}{4}\left(\mathrm{tr}(\mathbf{Q}^2)\right)^2. \tag{7}$$

Above, A, B, C are material parameters such that A, B, C are positive; K is a convenient constant to ensure $\psi \geq 0$. Stationary points of ψ are either uniaxial or isotropic $\mathbf{Q}$-tensors [52].

This potential was introduced to describe the vicinity of the isotropic-nematic phase transition, which is weakly first order. Therefore the eigenvalues of $\mathbf{Q}$ are small. However, the same potential is used to describe systems deep inside the nematic phase, while not providing for any constraint on the eigenvalues. It is known that they can leave their physically admissible range in some circumstances. For example, consideration of an elastically anisotropic phase $K_1 \neq K_3$ requires that $L_* \neq 0$. In this case, the energy $E[\mathbf{Q}]$ is unbounded below for any choice of physical parameters [31, 32], a divergence that is related to the absence of a constraint on the eigenvalues. The computational approach that we present here is precisely designed to remedy this problem.

3. Self Consistent Mean Field Theory

3.1. Macroscopic order parameter

We review the singular bulk potential introduced in [53, 31]. The goal is to have a bulk potential that correctly controls the eigenvalues of $\mathbf{Q} \in \boldsymbol{\Xi}$, where $\boldsymbol{\Xi}$ is the set of symmetric, traceless 3×3 matrices. Note that $\boldsymbol{\Xi}$ is spanned by a set of five basis matrices $\{\mathbf{E}^k\}_{k=1}^5$ [54].

The first step is to introduce a definition of the macroscopic order parameter (or mesoscopic field, under the assumption of local equilibrium), given by

$$\mathbf{Q} = \int_{S^2} \left(\mathbf{p} \otimes \mathbf{p} - \frac{1}{3}\mathbf{I} \right) \rho(\mathbf{p})\, dS(\mathbf{p}), \tag{8}$$

where $\rho \in \mathcal{P}$ is the equilibrium probability distribution of the LC molecules given by statistical mechanics, i.e.

$$\mathcal{P} := \left\{ \rho \in L^1(S^2; \mathbb{R}) \mid \ \rho \geq 0, \quad \int_{S^2} \rho(\mathbf{p})\, dS(\mathbf{p}) = 1 \right\}. \tag{9}$$

Note that $\mathbf{Q}$ as defined is a thermal average. Therefore the minimization discussed in Sec. 3.2 at fixed $\mathbf{Q}$ needs to be understood in a mean field sense. Note also that in the case of a non uniform configuration, we will assume that the same definition is valid so that an order parameter field $\mathbf{Q}(\mathbf{x})$ is defined from the local distribution $\rho(\mathbf{p}, \mathbf{x})$.

Equation (8) implies that the eigenvalues of $\mathbf{Q}$, denoted $\lambda_i \equiv \lambda_i(\mathbf{Q})$, satisfy

$$-\frac{1}{3} \leq \lambda_i(\mathbf{Q}) \leq \frac{2}{3}, \quad \text{for } i = 1, 2, 3, \qquad \sum_{i=1}^{3} \lambda_i(\mathbf{Q}) = 0. \tag{10}$$

In numerical work involving the Landau-de Gennes energy, equilibrium configurations of $\mathbf{Q}$ are obtained by energy minimization, where the energy functional $E(\mathbf{Q})$ is *independent* of any probability distribution of the underlying orientation of uniaxial molecules. In other words, (10) is not guaranteed. In contrast, the potential function defined below in Eq. (13) provides an energetic penalty so that the eigenvalues of $\mathbf{Q}$ satisfy the bounds in (10).

3.2. Self-consistent free energy

Let us define the entropy functional

$$S[\rho] = \int_{S^2} \rho(\mathbf{p}) \ln \rho(\mathbf{p})\, dS(\mathbf{p}), \tag{11}$$

and the intermolecular interaction kernel

$$K[\rho, \eta] = \int_{S^2} \int_{S^2} \left[(\mathbf{p} \cdot \mathbf{q})^2 - \frac{1}{3} \right] \rho(\mathbf{p}) \eta(\mathbf{q})\, dS(\mathbf{p})\, dS(\mathbf{q}), \tag{12}$$

where ρ and η are two probability distribution functions in $\mathcal{P}$. The Maier-Saupe Potential is defined as

$$I_{\mathrm{MS}}[\rho] = TS[\rho] - \kappa K[\rho, \rho], \tag{13}$$

where $T > 0$ is temperature, and $\kappa > 0$ is a constant (we have omitted the Boltzmann constant k_B). With this definition, I_{MS} reduces to the thermodynamic free energy when the distribution ρ is the corresponding equilibrium probability distribution.

One, however, proceeds differently. Given a value of $\mathbf{Q}$ (or locally, if a field $\mathbf{Q}(\mathbf{x})$ is specified), we minimize $I_{\mathrm{MS}}[\rho]$ over the space of probability distribution functions with the condition that $\mathbf{Q}$ is given by Eq. (8).

It is straightforward to write the interaction energy solely as a function of $\mathbf{Q}$. We have

$$\begin{aligned} K[\rho, \rho] &= \int_{S^2} \mathbf{q}^T \left(\int_{S^2} \left[\mathbf{p} \otimes \mathbf{p} - \frac{1}{3}\mathbf{I} \right] \rho(\mathbf{p})\, dS(\mathbf{p}) \right) \mathbf{q} \rho(\mathbf{q})\, dS(\mathbf{q}) \\ &= \int_{S^2} \mathbf{q}^T \mathbf{Q} \mathbf{q} \rho(\mathbf{q})\, dS(\mathbf{q}) = \mathbf{Q} : \int_{S^2} \left[\mathbf{q} \otimes \mathbf{q} - \frac{1}{3}\mathbf{I} \right] \rho(\mathbf{q})\, dS(\mathbf{q}) = \mathbf{Q} : \mathbf{Q} = |\mathbf{Q}|^2, \end{aligned} \tag{14}$$

where we used the fact that $\mathbf{Q}$ is traceless. Therefore, the energy term in the Maier-Saupe free energy of a given configuration $\mathbf{Q}$ is simply $-\kappa|\mathbf{Q}|^2$.

The computation of the entropy for fixed $\mathbf{Q}$ is more complex. As in other field theories, one needs to "invert" the relationship in (8), i.e., given $\mathbf{Q}$ find the corresponding ρ that provides this value of $\mathbf{Q}$ in equilibrium. Of course, this is ill-posed, so we must impose some additional conditions. We use a mean field assumption, according to which ρ minimizes $I_{\mathrm{MS}}[\rho]$ over the admissible set, and define the corresponding mean field free energy as

$$\begin{aligned} \psi(\mathbf{Q}) &:= \inf_{\rho \in \mathcal{A}_{\mathbf{Q}}} I_{\mathrm{MS}}[\rho], \\ &= T \inf_{\rho \in \mathcal{A}_{\mathbf{Q}}} S[\rho] - \kappa |\mathbf{Q}|^2, \end{aligned} \tag{15}$$

where the admissible set is

$$\mathcal{A}_{\mathbf{Q}} := \left\{ \rho \in \mathcal{P} \mid \mathbf{Q} = \int_{S^2} \left[\mathbf{p} \otimes \mathbf{p} - \frac{1}{3}\mathbf{I} \right] \rho(\mathbf{p})\, dS(\mathbf{p}) \right\}. \tag{16}$$

Since $\mathbf{Q}$ is fixed, we can focus on the entropy. Define

$$f(\mathbf{Q}) := \begin{cases} \inf_{\rho \in \mathcal{A}_{\mathbf{Q}}} S[\rho], & \text{if eigenvalues of } \mathbf{Q} \text{ satisfy (10)}, \\ +\infty, & \text{else.} \end{cases} \tag{17}$$

Then

$$\psi(\mathbf{Q}) = T f(\mathbf{Q}) - \kappa |\mathbf{Q}|^2. \tag{18}$$

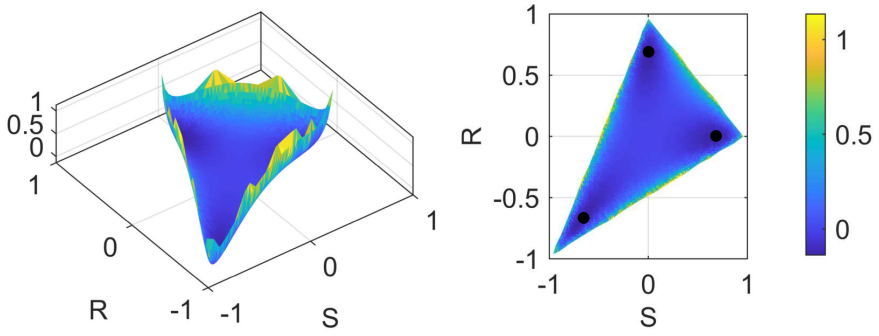

Figure 1: The bulk potential, Eq. (18), with $\mathbf{Q} = S(\mathbf{n}\otimes\mathbf{n} - (1/3)\mathbf{I}) + R(\mathbf{m}\otimes\mathbf{m} - (1/3)\mathbf{I})$ and $\kappa/T = 4$. The energy goes to infinity as $\mathbf{Q}$ approaches the physical bounds. For the chosen value of κ/T there are three minima that represent uniaxial states for each possible director direction which are highlighted with black dots.

Figure 1 shows plots of Eq. (18) for $\mathbf{Q}$ parameterized as

$$\mathbf{Q} = S\left(\mathbf{n}\otimes\mathbf{n} - \frac{1}{3}\mathbf{I}\right) + R\left(\mathbf{m}\otimes\mathbf{m} - \frac{1}{3}\mathbf{I}\right) \tag{19}$$

over the "physical triangle" as in [52]. For the plots we set $\kappa/T = 4$. As seen in the figure, when $\mathbf{Q}$ gets close to the physical bounds the bulk potential diverges. For this value of κ/T, there are three minima corresponding to uniaxial states where the director is $\mathbf{n}$, $\mathbf{m}$, or $\mathbf{n}\times\mathbf{m}$. For $\kappa/T < 3.4049$ there is a single minimum at $\mathbf{Q} = \mathbf{0}$ corresponding to the isotropic phase [42].

3.3. Properties

Before proceeding with the numerical algorithm, and for completeness, we begin by summarizing a few preliminary results, see [31].

Lemma 1. *For any $\mathbf{Q}\in\Xi$, such that $-1/3 < \lambda_i(\mathbf{Q}) < 2/3$ (for $i = 1,2,3$), the set $\mathcal{A}_\mathbf{Q}$ is non-empty.*

Proof. Given $\mathbf{Q}\in\Xi$, let $\mathbf{R}$ be the orthogonal matrix that diagonalizes $\mathbf{Q}$, i.e. $\mathbf{\Lambda} = \mathbf{R}^T\mathbf{Q}\mathbf{R}$, where $(\mathbf{\Lambda})_{ii} = \lambda_i(\mathbf{Q})$, for $i = 1,2,3$, where $2/3 > \lambda_1 \geq 0$, $-1/3 < \lambda_3 \leq 0$. Now define the following (generalized) function (singular measure)

$$\tilde{\rho}(\mathbf{p}) = \sum_{k=1}^{3}\left(\lambda_k + \frac{1}{3}\right)\frac{\delta(\mathbf{p}-\mathbf{e}_k) + \delta(\mathbf{p}+\mathbf{e}_k)}{2}, \quad \text{where} \quad \int_{S^2}\tilde{\rho}(\mathbf{p})\,dS(\mathbf{p}) = 1, \tag{20}$$

where $\delta(\cdot - \mathbf{a})$, for $\mathbf{a}\in S^2$, is the Dirac delta function on S^2 such that

$$\int_{S^2} g(\mathbf{p})\delta(\mathbf{p}-\mathbf{a})\,dS(\mathbf{p}) = g(\mathbf{a}). \tag{21}$$

Now let $X_{ij} := \int_{S^2} \left(\mathbf{p}\otimes\mathbf{p} - \frac{1}{3}\mathbf{I}\right)_{ij} \tilde{\rho}(\mathbf{p})\, dS(\mathbf{p})$, for $1 \le i,j \le 3$, and one can check that

$$X_{ii} = \lambda_i, \quad \text{for } i = 1,2,3, \quad \text{and} \quad X_{ij} = 0, \quad \text{for } i \neq j. \tag{22}$$

In other words, we have

$$\mathbf{\Lambda} = \int_{S^2} \left(\mathbf{p}\otimes\mathbf{p} - \frac{1}{3}\mathbf{I}\right) \tilde{\rho}(\mathbf{p})\, dS(\mathbf{p}), \tag{23}$$

i.e. it satisfies the constraint. Next, we replace $(\delta(\mathbf{p}-\mathbf{e}_k) + \delta(\mathbf{p}+\mathbf{e}_k))/2$ by a regularized version

$$\phi_k^\epsilon(\mathbf{p}) = \begin{cases} \frac{1}{2|A_\epsilon^1|}, & \text{if } \ |\mathbf{p}\cdot\mathbf{e}_k| \ge 1-\epsilon, \\ 0, & \text{if } \ |\mathbf{p}\cdot\mathbf{e}_k| < 1-\epsilon, \end{cases} \tag{24}$$

where $\pm A_\epsilon^k$ denotes the spherical cap at $\pm\mathbf{e}_k$ and $|A_\epsilon^1| = 2\pi\epsilon$ is the area of one of the two spherical caps over which $\phi_k^\epsilon \neq 0$, with $\epsilon > 0$ small. Now define a regularized version of (20):

$$\tilde{\rho}^\epsilon(\mathbf{p}) = a_0 \sum_{k=1}^{3} \left(\lambda_k + \frac{1}{3} + a_1\right) \phi_k^\epsilon(\mathbf{p}), \tag{25}$$

where $a_0 > 0$ and a_1 are constants. For convenience, define

$$r_i^k = \frac{1}{2|A_\epsilon^1|} \int_{+A_\epsilon^k \cup -A_\epsilon^k} p_i^2\, dS(\mathbf{p}), \quad r_i^i = 1 - O(\epsilon), \forall i, \quad r_i^k = O(\epsilon^2), \text{ for } i \neq k, \tag{26}$$

and note that $1 = \sum_{i=1} r_i^k$ for all $k = 1,2,3$, and symmetry implies

$$r_i^k = r_k^i, \quad \text{and} \quad r_k^i = r_t^i \ \text{ for all } i,k,t \ \text{ distinct}, \tag{27}$$

which implies that $r_k^k + 2r_k^i = 1$ whenever $i \neq k$. Now define $X_{ij}^\epsilon := \int_{S^2} \left(\mathbf{p}\otimes\mathbf{p} - \frac{1}{3}\mathbf{I}\right)_{ij} \tilde{\rho}^\epsilon(\mathbf{p})\, dS(\mathbf{p})$, for $1 \le i,j \le 3$, and compute:

$$\begin{aligned} X_{ii}^\epsilon &= a_0 \sum_{k=1}^{3} \left(\lambda_k + \frac{1}{3} + a_1\right) \frac{1}{2|A_\epsilon^1|} \int_{+A_\epsilon^k \cup -A_\epsilon^k} \left(p_i^2 - \frac{1}{3}\right) dS(\mathbf{p}) \\ &= a_0 \sum_{k=1}^{3} \left(\lambda_k + \frac{1}{3} + a_1\right) \left(r_i^k - \frac{1}{3}\right) \\ &= a_0 \sum_{k\neq i} \left(\lambda_k + \frac{1}{3} + a_1\right) \left(r_i^k - \frac{1}{3}\right) + a_0 \left(\lambda_i + \frac{1}{3} + a_1\right) \left(r_i^i - \frac{1}{3}\right). \end{aligned} \tag{28}$$

Since $r_i^i = r_1^1$ for all i, and $r_i^k = r_1^2$ for all $i \neq k$, we continue to simplify (28):

$$\begin{aligned} X_{ii}^{\epsilon} a_0^{-1} &= \left(r_1^2 - \frac{1}{3}\right) \sum_{k \neq i} \left(\lambda_k + \frac{1}{3} + a_1\right) + \left(\lambda_i + \frac{1}{3} + a_1\right)\left(r_1^1 - \frac{1}{3}\right) \\ &= \left(r_1^2 - \frac{1}{3}\right)\left[\frac{2}{3} - \lambda_i + 2a_1\right] + \left(\lambda_i + \frac{1}{3} + a_1\right)\left(r_1^1 - \frac{1}{3}\right) \\ &= \lambda_i \left(r_1^1 - r_1^2\right) + \left(\frac{1}{3} + a_1\right) \underbrace{\left(r_1^1 + 2r_1^2 - 1\right)}_{=0} \\ &= \lambda_i \left(r_1^1 - r_1^2\right). \end{aligned} \tag{29}$$

Thus, letting $a_0 := \left(r_1^1 - r_1^2\right)^{-1} = 1 + O(\epsilon)$, we get

$$X_{ii}^{\epsilon} = \lambda_i, \quad \text{for} \quad i = 1, 2, 3. \tag{30}$$

In addition, for $i \neq j$, we see that

$$X_{ij}^{\epsilon} = a_0 \sum_{k=1}^{3} \left(\lambda_k + \frac{1}{3} + a_1\right) \frac{1}{2|A_\epsilon^1|} \int_{+A_\epsilon^k \cup -A_\epsilon^k} p_i p_j \, dS(\mathbf{p}) = 0, \tag{31}$$

where the integral term drops by symmetry/cancellation. Note that (30) and (31) hold for any value of a_1. We must choose a_1 such that

$$\begin{aligned} 1 &= \int_{S^2} \tilde{\rho}^{\epsilon}(\mathbf{p}) \, dS(\mathbf{p}) = a_0 \sum_{k=1}^{3} \left(\lambda_k + \frac{1}{3} + a_1\right) = a_0 \left(1 + 3a_1\right), \\ \Rightarrow \quad a_1 &= \frac{1}{3}\left(\frac{1}{a_0} - 1\right) = O(\epsilon), \end{aligned} \tag{32}$$

where a_1 may be negative. Since $\lambda_k + 1/3 > 0$, choosing $\epsilon > 0$ sufficiently small (but fixed), we see that $\lambda_k + (1/3) + a_1 > 0$ for $k = 1, 2, 3$. Therefore, $\tilde{\rho}^{\epsilon}(\mathbf{p}) \geq 0$ for all $\mathbf{p}$, and $\tilde{\rho}^{\epsilon} \in \mathcal{P}$. Moreover,

$$\mathbf{\Lambda} = \int_{S^2} \left(\mathbf{p} \otimes \mathbf{p} - \frac{1}{3}\mathbf{I}\right) \tilde{\rho}^{\epsilon}(\mathbf{p}) \, dS(\mathbf{p}), \tag{33}$$

and $\tilde{\rho}^{\epsilon} \in \mathcal{A}_{\mathbf{\Lambda}}$. Finally, by rotating coordinates with $\mathbf{R}$, and defining $\hat{\rho}^{\epsilon}(\mathbf{R}\mathbf{p}) := \tilde{\rho}^{\epsilon}(\mathbf{p})$, (33) transforms into

$$\mathbf{Q} = \int_{S^2} \left(\hat{\mathbf{p}} \otimes \hat{\mathbf{p}} - \frac{1}{3}\mathbf{I}\right) \hat{\rho}^{\epsilon}(\hat{\mathbf{p}}) \, dS(\hat{\mathbf{p}}), \tag{34}$$

where $\hat{\rho}^{\epsilon} \in \mathcal{A}_{\mathbf{Q}}$. So $\mathcal{A}_{\mathbf{Q}}$ is non-empty. □

The following result lays out the main aspects of f needed.

Theorem 2. *Given* $\mathbf{Q}$ *with* $-1/3 < \lambda_i(\mathbf{Q}) < 2/3$ *(for* $i = 1, 2, 3$*), there exists a unique minimizer* $\rho^* \in \mathcal{A}_{\mathbf{Q}}$ *to the optimization problem in* (17)*. In other words,*

$$f(\mathbf{Q}) = \int_{S^2} \rho^*(\mathbf{p}) \ln \rho^*(\mathbf{p})\, dS(\mathbf{p}), \tag{35}$$

where

$$\rho^*(\mathbf{p}) = \frac{\exp\left(\mathbf{p}^T \mathbf{A} \mathbf{p}\right)}{Z(\mathbf{A})}, \quad Z(\mathbf{A}) = \int_{S^2} \exp\left(\mathbf{p}^T \mathbf{A} \mathbf{p}\right)\, dS(\mathbf{p}), \tag{36}$$

and $\mathbf{A} \in \mathbf{\Xi}$ *(symmetric, traceless) is the (unique) Lagrange multiplier for the constraint in* (16)*. Moreover,* $\mathbf{A}$ *satisfies the following non-linear equation, a requirement of mean field self-consistency:*

$$\frac{1}{Z(\mathbf{A})} \frac{\partial Z(\mathbf{A})}{\partial \mathbf{A}} : \mathbf{P} = \mathbf{Q} : \mathbf{P}, \quad \textit{for all } \mathbf{P} \in \mathbf{\Xi}. \tag{37}$$

Proof. **Step 1.** We show that the minimization problem is well-posed. From Lemma 1, we know $\mathcal{A}_{\mathbf{Q}}$ is non-empty. Moreover, the constraint in (16) is clearly convex, so $\mathcal{A}_{\mathbf{Q}}$ is a convex set. In addition, $S[\cdot]$ is a convex functional on $\mathcal{P}$, because $\rho \ln \rho$ is a (strictly) convex function of ρ. Hence, $S[\cdot]$ is weakly lower semi-continuous on $\mathcal{P}$. So, by standard theory from the calculus of variations, there exists a minimizer $\rho^* \in \mathcal{A}_{\mathbf{Q}}$, and it is unique by convexity.

Step 2. Derive the Euler-Lagrange equations that characterize the minimizer. We will mainly proceed formally, but this can be made more rigorous with similar arguments as in [55, Ch. 8]. In order to account for the constraint in $\mathcal{A}_{\mathbf{Q}}$, define the *Lagrangian*

$$\begin{aligned} L\left[\rho, \mathbf{A}\right] &:= S[\rho] + \mathbf{A} : \mathbf{C}\left[\rho\right] = \int_{S^2} \rho(\mathbf{p}) \ln \rho(\mathbf{p})\, dS(\mathbf{p}) + \mathbf{A} : \mathbf{C}\left[\rho\right], \\ \mathbf{C}\left[\rho\right] &:= \mathbf{Q} - \int_{S^2} \left(\mathbf{p} \otimes \mathbf{p} - \frac{1}{3}\mathbf{I}\right) \rho(\mathbf{p})\, dS(\mathbf{p}) \in \mathbf{\Xi}, \end{aligned} \tag{38}$$

where $\mathbf{A}$ is a constant matrix in $\mathbf{\Xi}$. In order to account for the other constraints of ρ being a probability measure, let us parameterize it:

$$\rho(\mathbf{p}) = \frac{e^{\omega(\mathbf{p})}}{Z(\omega)}, \quad \text{where} \quad Z(\omega) = \int_{S^2} e^{\omega(\mathbf{p})}\, dS(\mathbf{p}), \tag{39}$$

where $\omega : S^2 \to \mathbb{R} \cup \{-\infty\}$ is an "arbitrary" (measurable) function; thus, ρ is a probability measure for any ω. We list some perturbation formulas that will be useful later. Let $\omega_\epsilon = \omega + \epsilon\eta$, where $\epsilon > 0$ is small, and η is an arbitrary

measurable function (perturbation). Then, standard variational calculus gives

$$\begin{aligned}
&\delta_\omega(e^\omega)(\eta) := \frac{d}{d\epsilon}\Big|_{\epsilon=0} e^{\omega+\epsilon\eta} = \eta e^\omega, \quad \delta_\omega Z(\omega)(\eta) = \int_{S^2} \eta(\mathbf{p}) e^{\omega(\mathbf{p})}\, dS(\mathbf{p}), \\
&\delta_\omega\left(\frac{\omega}{Z(\omega)}\right)(\eta) = \frac{\eta}{Z(\omega)} - \frac{\omega}{(Z(\omega))^2}\delta_\omega Z(\omega)(\eta) = \frac{1}{Z(\omega)}\left(\eta - \omega\int_{S^2}\eta(\mathbf{p})\rho(\mathbf{p})\, dS(\mathbf{p})\right) = \frac{1}{Z(\omega)}\left(\eta - \omega\bar{\eta}\right), \\
&\delta_\omega\left(\frac{e^\omega}{Z(\omega)}\right)(\eta) = \frac{\eta e^\omega}{Z(\omega)} - \frac{e^\omega}{(Z(\omega))^2}\delta_\omega Z(\omega)(\eta) = \rho(\mathbf{p})\left(\eta(\mathbf{p}) - \bar{\eta}\right),
\end{aligned} \tag{40}$$

where $\bar{\eta} = \mathbb{E}_\rho[\eta]$ (the expected value with respect to ρ).

Step 3. Next, we derive the KKT conditions for the optimal solution of the problem, in terms of ω. So, we instead form the Lagrangian (38) in terms of ω: $L[\omega, \mathbf{A}] := S[\omega] + \mathbf{A} : \mathbf{C}[\omega]$. Computing the variation of the entropy, we have

$$\begin{aligned}
\delta_\omega S[\omega](\eta) &= \int_{S^2} \delta_\omega\left(\frac{e^\omega}{Z(\omega)}\right)(\eta)\left[\omega(\mathbf{p}) - \ln Z(\omega)\right] dS(\mathbf{p}) + \int_{S^2}\rho(\mathbf{p})\left[\eta(\mathbf{p}) - \frac{1}{Z(\omega)}\delta_\omega Z(\omega)(\eta)\right] dS(\mathbf{p}) \\
&= \int_{S^2}\rho(\mathbf{p})\left(\eta(\mathbf{p}) - \bar{\eta}\right)\left[\omega(\mathbf{p}) + 1 - \ln Z(\omega)\right] dS(\mathbf{p}) = \int_{S^2}\rho(\mathbf{p})\left(\eta(\mathbf{p}) - \bar{\eta}\right)\omega(\mathbf{p})\, dS(\mathbf{p}),
\end{aligned} \tag{41}$$

where the last equality is because of the definition of $\bar{\eta}$ and the fact that $+1 - \ln Z(\omega)$ is a constant. Note that ρ satisfies (39).

Next, note that

$$\mathbf{A} : \mathbf{C}[\omega] = \mathbf{A} : \mathbf{Q} - \int_{S^2} \mathbf{p}^T\mathbf{A}\mathbf{p}\frac{e^{\omega(\mathbf{p})}}{Z(\omega)}\, dS(\mathbf{p}). \tag{42}$$

Hence, the first variation of the constraint gives

$$\delta_\omega(\mathbf{A} : \mathbf{C}[\omega])(\eta) = -\int_{S^2}\mathbf{p}^T\mathbf{A}\mathbf{p}\,\delta_\omega\left(\frac{e^\omega}{Z(\omega)}\right)(\eta)\, dS(\mathbf{p}) = -\int_{S^2}\mathbf{p}^T\mathbf{A}\mathbf{p}\,\rho(\mathbf{p})\left(\eta(\mathbf{p}) - \bar{\eta}\right) dS(\mathbf{p}). \tag{43}$$

The first KKT condition is given by $\delta_\omega L[\omega, \mathbf{A}](\eta) = 0$, for all admissible η. Therefore, by the above calculations, we obtain

$$0 = \delta_\omega L[\omega, \mathbf{A}](\eta) = \int_{S^2}\left[\omega(\mathbf{p}) - \mathbf{p}^T\mathbf{A}\mathbf{p}\right]\rho(\mathbf{p})\left(\eta(\mathbf{p}) - \bar{\eta}\right) dS(\mathbf{p}), \tag{44}$$

for all admissible η. This implies that $\omega(\mathbf{p}) - \mathbf{p}^T\mathbf{A}\mathbf{p} = c$, where c is any constant. So, from (39), we find

$$\rho(\mathbf{p}) = e^c\frac{\exp\left(\mathbf{p}^T\mathbf{A}\mathbf{p}\right)}{Z(\omega)} = \frac{\exp\left(\mathbf{p}^T\mathbf{A}\mathbf{p}\right)}{Z(\mathbf{A})}, \tag{45}$$

where the e^c term cancels out. Since the minimizer is unique, we have proven (36). The second KKT condition simply recovers the constraint $\mathbf{0} = \partial L[\omega, \mathbf{A}]/\partial\mathbf{A} = \mathbf{C}[\omega]$.

Step 4. Finally, the last step in the inversion is an equation to determine $\mathbf{A} \in \mathbf{\Xi}$. Starting from the relation $Z(\mathbf{A}) = \int_{S^2} \exp\left(\mathbf{p}^T \mathbf{A} \mathbf{p}\right) \, dS(\mathbf{p})$, we first differentiate with respect $\mathbf{A}$ but in the direction of general symmetric matrices, not necessarily trace free:

$$\begin{aligned}
\frac{\partial Z(\mathbf{A})}{\partial \mathbf{A}} &= \int_{S^2} \frac{\partial}{\partial \mathbf{A}} \left(\mathbf{p}^T \mathbf{A} \mathbf{p}\right) \exp\left(\mathbf{p}^T \mathbf{A} \mathbf{p}\right) \, dS(\mathbf{p}) = \int_{S^2} (\mathbf{p} \otimes \mathbf{p}) \exp\left(\mathbf{p}^T \mathbf{A} \mathbf{p}\right) \, dS(\mathbf{p}) \\
&= \int_{S^2} \left(\mathbf{p} \otimes \mathbf{p} - \frac{1}{3}\mathbf{I}\right) \exp\left(\mathbf{p}^T \mathbf{A} \mathbf{p}\right) \, dS(\mathbf{p}) + \frac{1}{3}\mathbf{I} \int_{S^2} \exp\left(\mathbf{p}^T \mathbf{A} \mathbf{p}\right) \, dS(\mathbf{p}) \\
&= Z(\mathbf{A}) \left[\int_{S^2} \left(\mathbf{p} \otimes \mathbf{p} - \frac{1}{3}\mathbf{I}\right) \rho(\mathbf{p}) \, dS(\mathbf{p}) + \frac{1}{3}\mathbf{I}\right] = Z(\mathbf{A}) \left[\mathbf{Q} + \frac{1}{3}\mathbf{I}\right],
\end{aligned} \tag{46}$$

where ρ satisfies (45). Thus, the multiplier $\mathbf{A}$ satisfies the following equation

$$\frac{1}{Z(\mathbf{A})} \frac{\partial Z(\mathbf{A})}{\partial \mathbf{A}} = \mathbf{Q} + \frac{1}{3}\mathbf{I}. \tag{47}$$

Dotting (47) with an arbitrary "test" function in $\mathbf{\Xi}$, we get (37). □

We will also make use of these results for f. Note that the partition function (39) is a single particle partition function obtained by integration over $\mathbf{p} \in S^2$, but with *specified* values of the Lagrange multiplier $\mathbf{A}$. The fact that it simply involves a quadratic form of $\mathbf{p}$ originates from the form of the constrain (8). In the mean field approximation considered, given $\mathbf{Q}$ there is a unique $\mathbf{A}$, defined by (47), so that the corresponding ρ in (39) gives as average precisely $\mathbf{Q}$.

The following result illustrates additional properties of $f(\mathbf{Q})$, including the simultaneous diagonalization of $\mathbf{Q}$ and $\mathbf{A}$, which can be useful for numerical implementation purposes.

Corollary 3. *The function $f(\mathbf{Q})$ is a strictly convex function of $\mathbf{Q}$. In addition, any $\mathbf{Q} \in \mathbf{\Xi}$, and the corresponding unique $\mathbf{A}$ coming from solving the constrained minimization problem in Theorem 2, are diagonalized by the* same *orthogonal matrix $\mathbf{R}$, i.e.*

$$\mathbf{\Lambda} = \mathbf{R}^T \mathbf{Q} \mathbf{R}, \quad \mathbf{\Pi} = \mathbf{R}^T \mathbf{A} \mathbf{R}, \tag{48}$$

where $\mathbf{\Lambda} = \operatorname{diag}(\lambda_1, \lambda_2, \lambda_3)$ and $\mathbf{\Pi} = \operatorname{diag}(\pi_1, \pi_2, \pi_3)$, where $\{\pi_i\}_{i=1}^3$ are the eigenvalues of $\mathbf{A}$.

Moreover, the Lagrange multiplier $\mathbf{A}$ can be characterized as the optimal solution of the dual problem. In other words, define

$$W(\mathbf{A}) := \ln\left(Z(\mathbf{A})\right) - \mathbf{Q} : \mathbf{A}, \tag{49}$$

where $W(\cdot) : \mathbf{\Xi} \to \mathbb{R}$ is a strictly convex function (but not uniformly strictly convex). Then, the optimal Lagrange multiplier $\mathbf{A}$ from Theorem 2 is the unique minimizer of (49) *over the set of symmetric, traceless matrices, i.e. an unconstrained minimization problem.*

Proof. **Convexity.** Let $\mathbf{Q}_0, \mathbf{Q}_1 \in \mathbf{\Xi}$ with eigenvalues satisfying (10), and let ρ_i be the minimizer in (35) corresponding to $\mathbf{Q}_i$, for $i = 0, 1$. Set $\mathbf{Q}(t) = \mathbf{Q}_0(1-t) + \mathbf{Q}_1 t$ for all $t \in [0,1]$, and also define $\rho(\cdot, t) := \rho_0(\cdot)(1-t) + \rho_1(\cdot)t$. Then, since $S[\rho]$ is a strictly convex functional of ρ, for all $0 < t < 1$ we have

$$\begin{aligned} f(\mathbf{Q}(t)) &= \min_{\rho \in \mathcal{A}_{\mathbf{Q}(t)}} S[\rho] \leq S[\rho(\cdot,t)] < S[\rho_0](1-t) + S[\rho_1]t \\ &= \left(\min_{\rho \in \mathcal{A}_{\mathbf{Q}_0}} S[\rho] \right)(1-t) + \left(\min_{\rho \in \mathcal{A}_{\mathbf{Q}_1}} S[\rho] \right) t = f(\mathbf{Q}_0)(1-t) + f(\mathbf{Q}_1)t, \end{aligned} \tag{50}$$

which verifies the strict convexity of $f(\cdot)$.

Simultaneous diagonalization. Given $\mathbf{Q}$, let $\mathbf{A}$ and ρ be the optimal solution of the constrained minimization problem, and let $\mathbf{R}$ be the orthogonal matrix such that $\mathbf{\Pi} = \mathbf{R}^T \mathbf{A} \mathbf{R}$ where $\mathbf{\Pi}$ is a diagonal matrix. Then, using the change of variable $\mathbf{p} = \mathbf{R}\mathbf{q}$, we get

$$\begin{aligned} Z(\mathbf{A})\mathbf{Q} &= \int_{S^2} \left(\mathbf{p}\mathbf{p}^T - \frac{1}{3}\mathbf{I} \right) \exp\left(\mathbf{p}^T \mathbf{A} \mathbf{p} \right) \, dS(\mathbf{p}) = \int_{S^2} \left(\mathbf{R}\mathbf{q}\mathbf{q}^T\mathbf{R}^T - \frac{1}{3}\mathbf{R}\mathbf{R}^T \right) \exp\left(\mathbf{q}^T \mathbf{R}^T \mathbf{A} \mathbf{R} \mathbf{q} \right) \, dS(\mathbf{q}) \\ &= \mathbf{R} \left[\int_{S^2} \left(\mathbf{q}\mathbf{q}^T - \frac{1}{3}\mathbf{I} \right) \exp\left(\sum_{i=1}^{3} \pi_i q_i^2 \right) \, dS(\mathbf{q}) \right] \mathbf{R}^T, \end{aligned} \tag{51}$$

i.e.

$$\mathbf{R}^T \mathbf{Q} \mathbf{R} = \frac{1}{Z(\mathbf{A})} \int_{S^2} \left(\mathbf{q}\mathbf{q}^T - \frac{1}{3}\mathbf{I} \right) \exp\left(\sum_{i=1}^{3} \pi_i q_i^2 \right) \, dS(\mathbf{q}). \tag{52}$$

Now, note that for $i \neq j$, there holds

$$0 = \int_{S^2} \underbrace{q_i q_j}_{\text{odd}} \underbrace{\exp\left(\sum_{i=1}^{3} \pi_i q_i^2 \right)}_{\text{even}} \, dS(\mathbf{q}). \tag{53}$$

That means $\mathbf{R}^T\mathbf{Q}\mathbf{R}$ must be diagonal. Since matrix diagonalization (with orthogonal matrices) is unique, $\mathbf{R}^T\mathbf{Q}\mathbf{R} \equiv \mathbf{\Lambda}$.

The dual minimization problem. Let $\mathbf{A}^*$ be the optimal Lagrange multiplier from (37); it is clear that $\mathbf{A}^*$ solves the first order condition for (49):

$$0 = \frac{\partial W(\mathbf{A})}{\partial \mathbf{A}} : \mathbf{P} = \frac{1}{Z(\mathbf{A})} \frac{\partial Z(\mathbf{A})}{\partial \mathbf{A}} : \mathbf{P} - \mathbf{Q} : \mathbf{P}, \quad \text{for all } \mathbf{P} \in \mathbf{\Xi}. \tag{54}$$

Next, we compute the Hessian of $W(\mathbf{A})$ for any $\mathbf{A} \in \mathbf{\Xi}$:

$$\mathbf{T} : \frac{\partial^2 W(\mathbf{A})}{\partial \mathbf{A}^2} : \mathbf{P} = \frac{1}{Z(\mathbf{A})} \mathbf{T} : \frac{\partial^2 Z(\mathbf{A})}{\partial \mathbf{A}^2} : \mathbf{P} - \frac{1}{(Z(\mathbf{A}))^2} \left(\frac{\partial Z(\mathbf{A})}{\partial \mathbf{A}} : \mathbf{T} \right) \left(\frac{\partial Z(\mathbf{A})}{\partial \mathbf{A}} : \mathbf{P} \right), \tag{55}$$

where

$$\frac{1}{Z(\mathbf{A})}\frac{\partial Z(\mathbf{A})}{\partial \mathbf{A}} : \mathbf{P} = \int_{S^2} \mathbf{p}^T\mathbf{P}\mathbf{p}\,\rho(\mathbf{p})\,dS(\mathbf{p}) = \mathbb{E}_\rho[\mathbf{p}^T\mathbf{P}\mathbf{p}],$$
$$\frac{1}{Z(\mathbf{A})}\mathbf{T} : \frac{\partial^2 Z(\mathbf{A})}{\partial \mathbf{A}^2} : \mathbf{P} = \int_{S^2} \left(\mathbf{p}^T\mathbf{T}\mathbf{p}\right)\left(\mathbf{p}^T\mathbf{P}\mathbf{p}\right)\rho(\mathbf{p})\,dS(\mathbf{p}) = \mathbb{E}_\rho[\left(\mathbf{p}^T\mathbf{T}\mathbf{p}\right)\left(\mathbf{p}^T\mathbf{P}\mathbf{p}\right)], \tag{56}$$

for all $\mathbf{P}, \mathbf{T} \in \mathbf{\Xi}$; note that $\mathbb{E}_\rho[\cdot]$ is the expected value with respect to ρ, which is determined by $\mathbf{A}$. To show strict convexity, we must verify that $\partial^2_{\mathbf{A}} W(\mathbf{A})$ is positive definite for all $\mathbf{A}$:

$$\mathbf{P} : \frac{\partial^2 W(\mathbf{A})}{\partial \mathbf{A}^2} : \mathbf{P} = \mathbb{E}_\rho[\left(\mathbf{p}^T\mathbf{P}\mathbf{p}\right)^2] - \left(\mathbb{E}_\rho[\mathbf{p}^T\mathbf{P}\mathbf{p}]\right)^2 = \mathbb{E}_\rho[\left(\mathbf{p}^T\mathbf{P}\mathbf{p} - \mathbb{E}_\rho[\mathbf{p}^T\mathbf{P}\mathbf{p}]\right)^2], \tag{57}$$

which is the covariance of $\mathbf{p}^T\mathbf{P}\mathbf{p}$ with respect to ρ (which depends on $\mathbf{A}$) and is always positive semi-definite. If (57) were identically zero, then that would imply that some marginal distribution of ρ is a Dirac delta. But this is not possible given the form of ρ in (45) so long as $\mathbf{A}$ is finite. Therefore, $\frac{\partial^2 W(\mathbf{A})}{\partial \mathbf{A}^2}$ is positive definite for all $\mathbf{A} \in \mathbf{\Xi}$ such that $|\mathbf{A}| < \infty$. This means that $W(\cdot)$ is strictly convex. □

4. Minimizing the Landau-de Gennes Energy

The free energy minimization of the self consistent free energy (18) shares many elements with minimization procedures of the Landau-de Gennes free energy. We summarize known results concerning the later here, and emphasize the differences with the proposed method.

4.1. Existence of a Minimizer

The admissible space for $\mathbf{Q}$ when seeking a minimizer is

$$\mathbb{V}(\mathbf{P}) := \left\{\mathbf{Q} \in H^1(\Omega; \mathbf{\Xi}) \mid \mathbf{Q}|_{\Gamma_D} = \mathbf{P}\right\}, \tag{58}$$

where $\mathbf{P} \in H^1(\Omega; \mathbf{\Xi})$. Note that $\mathbf{\Xi}$ is spanned by a set of five orthonormal basis matrices $\{\mathbf{E}^k\}_{k=1}^5$. The set $\Gamma_D \subset \Gamma$ is where strong anchoring is imposed, i.e. $\mathbf{Q}|_\Gamma = \mathbf{Q}_D \in H^1(\Gamma; \mathbf{\Xi})$, where $\psi(\mathbf{Q}_D(\mathbf{x})) < \infty$ for all $\mathbf{x} \in \Gamma$. The weak anchoring function $\mathbf{Q}_\Gamma$ is taken in $L^2(\Gamma; \mathbf{\Xi})$, with $\psi(\mathbf{Q}_\Gamma(\mathbf{x})) < \infty$ for all $\mathbf{x} \in \Gamma$. The minimization problem for the LdG energy functional (1) is

$$\min_{\mathbf{Q} \in \mathbb{V}(\mathbf{Q}_D)} E[\mathbf{Q}], \tag{59}$$

Existence of a minimizer requires the energy to be bounded from below. The following theorem [36, Lem. 4.1] establishes this result for the L_1, L_2, and L_3 terms only.

Theorem 4. *Let $a(\cdot,\cdot) : H^1(\Omega;\boldsymbol{\Xi}) \times H^1(\Omega;\boldsymbol{\Xi}) \to \mathbb{R}$ be the symmetric bilinear form defined by*

$$a(\mathbf{P},\mathbf{T}) = \int_\Omega L_1 \nabla\mathbf{P} \vdots \nabla\mathbf{T} + L_2(\nabla\cdot\mathbf{P})\cdot(\nabla\cdot\mathbf{T}) + L_3(\nabla\mathbf{P})^T \vdots \nabla\mathbf{T}\, d\mathbf{x}. \quad (60)$$

Then $a(\cdot,\cdot)$ is bounded. If L_1, L_2, L_3 satisfy

$$0 < L_1, \quad -L_1 < L_3 < 2L_1, \quad -\frac{3}{5}L_1 - \frac{1}{10}L_3 < L_2, \quad (61)$$

then there is a constant $C > 0$ such that $a(\mathbf{P},\mathbf{P}) \geq C|\mathbf{P}|^2_{H^1(\Omega)}$ for all $\mathbf{P} \in H^1(\Omega)$. Moreover, if $|\Gamma_D| > 0$, then there is a constant $C' > 0$ such that $a(\mathbf{P},\mathbf{P}) \geq C'\|\mathbf{P}\|^2_{H^1(\Omega)}$ for all $\mathbf{P} \in \mathbb{V}(\mathbf{0})$.

We also have the bilinear form $b(\cdot,\cdot) : H^1(\Omega;\boldsymbol{\Xi}) \times H^1(\Omega;\boldsymbol{\Xi}) \to \mathbb{R}$ and trilinear form $c(\cdot,\cdot;\cdot) : H^1(\Omega;\boldsymbol{\Xi}) \times H^1(\Omega;\boldsymbol{\Xi}) \times H^1(\Omega;\boldsymbol{\Xi}) \to \mathbb{R}$ accounting for the L_4 and L_* terms:

$$b(\mathbf{P},\mathbf{T}) = \frac{L_4}{2}\int_\Omega \nabla\mathbf{P} \vdots (\mathbf{e}\cdot\mathbf{T}) + \nabla\mathbf{T} \vdots (\mathbf{e}\cdot\mathbf{P})\, d\mathbf{x}, \quad (62)$$

$$\begin{aligned} c(\mathbf{T},\mathbf{P};\mathbf{Q}) = \frac{L_*}{2}\int_\Omega \Big\{ &\nabla\mathbf{P} \vdots [(\mathbf{T}\cdot\nabla)\mathbf{Q}] + \nabla\mathbf{P} \vdots [(\mathbf{Q}\cdot\nabla)\mathbf{T}] \\ &+\nabla\mathbf{T} \vdots [(\mathbf{P}\cdot\nabla)\mathbf{Q}] + \nabla\mathbf{T} \vdots [(\mathbf{Q}\cdot\nabla)\mathbf{P}] \\ &+\nabla\mathbf{Q} \vdots [(\mathbf{P}\cdot\nabla)\mathbf{T}] + \nabla\mathbf{Q} \vdots [(\mathbf{T}\cdot\nabla)\mathbf{P}] \Big\} d\mathbf{x}. \end{aligned} \quad (63)$$

Next, consider the following sub-part of the energy (1):

$$\begin{aligned} \widetilde{E}[\mathbf{Q}] &:= \int_\Omega \mathcal{W}(\mathbf{Q},\nabla\mathbf{Q})\, d\mathbf{x} + \frac{1}{\epsilon^2}\int_\Omega \psi(\mathbf{Q})\, d\mathbf{x}, \\ &\equiv \frac{1}{2}a(\mathbf{Q},\mathbf{Q}) + \frac{1}{2}b(\mathbf{Q},\mathbf{Q}) + \frac{1}{6}c(\mathbf{Q},\mathbf{Q};\mathbf{Q}) + \frac{1}{\epsilon^2}\int_\Omega \psi(\mathbf{Q})\, d\mathbf{x}. \end{aligned} \quad (64)$$

Combining Theorem 4 with the form of the energy in (1) and other basic results (see [36, Lem. 4.2, Thm. 4.3] for instance) we arrive at the following result.

Theorem 5 (existence of a minimizer)**.** *Suppose that $\mathbf{Q}_D$ and Γ_D are defined as above and that χ is a bounded linear functional on $\mathbb{V}(\mathbf{Q}_D)$. Let $\widetilde{E}$ be given by* (64)*, where ψ is given by* (18)*. Furthermore, assume $T > 0$, let L_4 be bounded, and assume that*

$$\widetilde{L}_1 := L_1 - \max\left(\frac{L_*}{3}, -\frac{3}{2}L_*\right), \quad (65)$$

and $\widetilde{L}_1$, L_2, L_3 satisfy (61) *with L_1 replaced by $\widetilde{L}_1$. Then $\widetilde{E}$ has a minimizer in the space $\mathbb{V}(\mathbf{Q}_D)$, whose eigenvalues are* strictly within *the physical limits* (10) *almost everywhere. Furthermore, E in* (1)*, with ψ given by* (18)*, has a minimizer in $\mathbb{V}(\mathbf{Q}_D)$, whose eigenvalues are* strictly within *the physical limits* (10) *almost everywhere.*

Proof. When $L_4 = L_* = 0$, the result follows from [36, Lem. 4.2, Thm. 4.3]. Otherwise, consider the case where L_* is positive (the negative case is similar). Consider the constrained admissible set

$$\mathcal{A} := \{\mathbf{Q} \in \mathbb{V}(\mathbf{Q}_D) \mid -1/3 \leq \lambda_i(\mathbf{Q}) \leq 2/3, \text{ for } i = 1, 2, 3\}, \tag{66}$$

and note that $\mathcal{A}$ is a closed, convex set. Since the minimum eigenvalue of $L_1\mathbf{I} + L_*\mathbf{Q}$ (on $\mathcal{A}$) is $\widetilde{L}_1$, using Theorem 4, we have that $\widetilde{E}$ satisfies the bound

$$\begin{aligned}\widetilde{E}[\mathbf{Q}] &\geq \frac{1}{2}\int_\Omega \widetilde{L}_1|\nabla\mathbf{Q}|^2 + L_2(\nabla\cdot\mathbf{Q})^2 + L_3(\nabla\mathbf{Q})^T \vdots \nabla\mathbf{Q}\, d\mathbf{x} \\ &\quad + \frac{L_4}{2}\int_\Omega \nabla\mathbf{Q} \vdots (\mathbf{e}\cdot\mathbf{Q})\, d\mathbf{x} + \frac{1}{\epsilon^2}\int_\Omega \psi(\mathbf{Q})\, d\mathbf{x} \\ &\geq \frac{C}{2}\int_\Omega |\nabla\mathbf{Q}|^2\, d\mathbf{x} + \frac{L_4}{2}\int_\Omega \nabla\mathbf{Q} \vdots (\mathbf{e}\cdot\mathbf{Q})\, d\mathbf{x} + \frac{1}{\epsilon^2}\int_\Omega \psi(\mathbf{Q})\, d\mathbf{x},\end{aligned} \tag{67}$$

for all $\mathbf{Q} \in \mathcal{A}$, for some constant $C > 0$. Furthermore, one can show

$$\widetilde{E}[\mathbf{Q}] \geq \frac{1}{2}(C - \zeta_0)\int_\Omega |\nabla\mathbf{Q}|^2\, d\mathbf{x} - \frac{C'}{\zeta_0}\int_\Omega |\mathbf{Q}|^2\, d\mathbf{x} + \frac{1}{\epsilon^2}\int_\Omega \psi(\mathbf{Q})\, d\mathbf{x}, \tag{68}$$

for any $\zeta_0 > 0$ where $C' > 0$ is some bounded constant. Choosing $\zeta_0 = C/2$, we get

$$\widetilde{E}[\mathbf{Q}] \geq \frac{C}{4}\int_\Omega |\nabla\mathbf{Q}|^2\, d\mathbf{x} + \frac{1}{\epsilon^2}\int_\Omega \widetilde{\psi}(\mathbf{Q})\, d\mathbf{x}, \tag{69}$$

where $\widetilde{\psi}(\mathbf{Q}) := Tf(\mathbf{Q}) - (\kappa + 2\epsilon^2 C'/C)|\mathbf{Q}|^2$. Thus, $\widetilde{E}[\mathbf{Q}]$ is clearly bounded below by a coercive energy on $\mathcal{A}$. By standard calculus of variations [56, 57], there exists a minimizer, $\widetilde{\mathbf{Q}}$, of $\widetilde{E}[\cdot]$ in $\mathcal{A}$. Moreover, $f(\widetilde{\mathbf{Q}}) < \infty$ almost everywhere, meaning the eigenvalues of $\widetilde{\mathbf{Q}}$ are strictly within the physical limits almost everywhere. The same holds true for $E[\cdot]$. □

4.2. Gradient Flow

We look for an energy minimizer using a gradient flow strategy [40, 37, 41, 35] applied to the energy (1). Let t represent "time" and suppose that $\mathbf{Q} \equiv \mathbf{Q}(\mathbf{x}, t)$ satisfies an evolution equation such that $\lim_{t\to\infty} \mathbf{Q}(\cdot, t) =: \mathbf{Q}_*$ is a local minimizer of E, where $\mathbf{Q}(\mathbf{x}, 0) = \mathbf{Q}_0$, and $\mathbf{Q}_0 \in \mathbb{V}(\mathbf{Q}_D)$ is the initial guess for the minimizer. The tensor $\mathbf{Q}(\cdot, t)$ evolves according to the following $L^2(\Omega)$ gradient flow:

$$(\partial_t\mathbf{Q}(\cdot, t), \mathbf{P}) = -\delta_{\mathbf{Q}}E[\mathbf{Q}; \mathbf{P}], \quad \forall \mathbf{P} \in \mathbb{V}(\mathbf{0}), \tag{70}$$

where $(\cdot, \cdot)$ is the L^2 inner product over Ω. Formally, the solution of (70) will converge to $\mathbf{Q}_*$.

Remark 6. *If ψ is the Landau-de Gennes bulk potential in* (7)*, then* (70) *is essentially a tensor-valued Allen-Cahn equation. By the standard theory of parabolic PDEs [58, 59], it has a unique solution. The same result also holds when ψ is the singular bulk potential.*

We use a numerical scheme for approximating (70) by first discretizing in time by minimizing movements [60]. Let $\mathbf{Q}_k(\mathbf{x}) \approx \mathbf{Q}(\mathbf{x}, k\delta t)$, where $\delta t > 0$ is a finite time-step, and k is the time index. Then (70) becomes a sequence of variational problems. Given $\mathbf{Q}_k$, find $\mathbf{Q}_{k+1} \in \mathbb{V}(\mathbf{Q}_D)$ such that

$$\left(\frac{\mathbf{Q}_{k+1} - \mathbf{Q}_k}{\delta t}, \mathbf{P}\right) = -\delta_{\mathbf{Q}} E[\mathbf{Q}_{k+1}; \mathbf{P}], \quad \forall \mathbf{P} \in \mathbb{V}(\mathbf{0}), \tag{71}$$

which is equivalent to

$$\mathbf{Q}_{k+1} = \underset{\mathbf{Q} \in \mathbb{V}(\mathbf{Q}_D)}{\arg\min}\ F(\mathbf{Q}), \quad F(\mathbf{Q}) := \frac{1}{2\delta t}\|\mathbf{Q} - \mathbf{Q}_k\|^2_{L^2(\Omega)} + E[\mathbf{Q}], \tag{72}$$

and yields the useful property $F(\mathbf{Q}_{k+1}) \leq F(\mathbf{Q}_k)$. However, (71) is a *fully-implicit* equation and requires an iterative solution because of the non-linearities in $\mathcal{W}(\mathbf{Q}, \nabla\mathbf{Q})$ and $\psi(\mathbf{Q})$. As in the Landau-de Gennes case, $\psi(\mathbf{Q})$ is non-convex [42], so that we adopt a *convex splitting* method [61, 41, 62]. Setting $\psi_c(\mathbf{Q}) = Tf(\mathbf{Q})$ and $\psi_e(\mathbf{Q}) = \kappa|\mathbf{Q}|^2$, we see that (18) already has the form of a convex splitting:

$$\psi(\mathbf{Q}) \equiv \psi_c(\mathbf{Q}) - \psi_e(\mathbf{Q}), \tag{73}$$

i.e. ψ_c and ψ_e are convex functions of $\mathbf{Q}$.

In computing (71), we treat ψ_c implicitly and ψ_e explicitly. Therefore, (71) becomes the following. Given $\mathbf{Q}_k$, find $\mathbf{Q}_{k+1} \in \mathbb{V}(\mathbf{Q}_D)$ such that

$$\begin{aligned}
&\left(\frac{\mathbf{Q}_{k+1} - \mathbf{Q}_k}{\delta t}, \mathbf{P}\right) + a\left(\mathbf{Q}_{k+1}, \mathbf{P}\right) + b\left(\mathbf{Q}_{k+1}, \mathbf{P}\right) + c\left(\mathbf{Q}_{k+1}, \mathbf{P}; \mathbf{Q}_{k+1}\right) \\
&\frac{1}{\epsilon^2}\int_\Omega \frac{\partial \psi_c(\mathbf{Q}_{k+1})}{\partial \mathbf{Q}} : \mathbf{P}\, d\mathbf{x} + \eta_\Gamma \int_\Gamma \frac{\partial f_\Gamma(\mathbf{Q}_{k+1})}{\partial \mathbf{Q}} : \mathbf{P}\, dS(\mathbf{x}) \\
&= \frac{1}{\epsilon^2}\int_\Omega \frac{\partial \psi_e(\mathbf{Q}_k)}{\partial \mathbf{Q}} : \mathbf{P}\, d\mathbf{x} + \int_\Omega \frac{\partial \chi(\mathbf{Q}_k)}{\partial \mathbf{Q}} : \mathbf{P}\, d\mathbf{x}, \quad \forall \mathbf{P} \in \mathbb{V}(\mathbf{0}),
\end{aligned} \tag{74}$$

where the right-hand-side of (74) is completely explicit. We then apply Newton's method to solving (74).

Next, we approximate (74) by a finite element method, so we introduce some basic notation and assumptions in that regard. We assume that $\Omega \subset \mathbb{R}^3$ is discretized by a conforming shape regular triangulation $\mathcal{T}_h = \{T_i\}$ consisting of simplices, i.e. we define $\Omega_h := \cup_{T \in \mathcal{T}_h} T$. Furthermore, we define the space of continuous piecewise linear functions on Ω_h:

$$\mathbb{M}_h(\Omega_h) := \left\{ v \in C^0(\Omega_h) \mid v|_T \in \mathcal{P}_1(T),\ \forall T \in \mathcal{T}_h \right\}, \tag{75}$$

where $\mathcal{P}_k(T)$ is the space of polynomials of degree $\leq k$ on T.

We discretize (74) by a $\mathcal{P}_1$ approximation of the $\mathbf{Q}$ variable denoted $\mathbf{Q}_h$. To this end, define

$$\mathbb{S}_h(\Omega_h) := \left\{ \mathbf{P} \in C^0(\Omega_h; \mathbf{\Xi}) \mid \mathbf{P} = \sum_{i=1}^{5} q_{i,h}\mathbf{E}^i,\ q_{i,h} \in \mathbb{M}_h(\Omega_h), 1 \leq i \leq 5 \right\}, \tag{76}$$

and let $\mathbf{Q}_h \in \mathbb{S}_h(\Omega_h)$. Thus, $\mathbf{Q}_h = \sum_{i=1}^{5} q_{i,h}\mathbf{E}^i$, and $\mathbf{Q}_h \in H^1(\Omega;\mathbf{\Xi})$.

The fully discrete L^2-gradient flow now follows from (74), which we explicitly state. Given $\mathbf{Q}_{h,k}$, find $\mathbf{Q}_{h,k+1} \in \mathbb{S}_h(\Omega_h) \cap \mathbb{V}(\mathcal{I}_h\mathbf{Q}_D)$, where $\mathcal{I}_h$ denotes the Lagrange interpolation operator, such that

$$\begin{aligned}
&\left(\frac{\mathbf{Q}_{h,k+1}-\mathbf{Q}_{h,k}}{\delta t},\mathbf{P}\right) + a\left(\mathbf{Q}_{h,k+1},\mathbf{P}\right) + b\left(\mathbf{Q}_{h,k+1},\mathbf{P}\right) + c\left(\mathbf{Q}_{h,k+1},\mathbf{P};\mathbf{Q}_{h,k+1}\right)\\
&\frac{1}{\epsilon^2}\int_\Omega \mathcal{I}_h\left(\frac{\partial\psi_c(\mathbf{Q}_{h,k+1})}{\partial\mathbf{Q}}\right) : \mathbf{P}\,d\mathbf{x} + \eta_\Gamma\int_\Gamma \frac{\partial f_\Gamma(\mathbf{Q}_{h,k+1})}{\partial\mathbf{Q}} : \mathbf{P}\,dS(\mathbf{x})\\
&= \frac{1}{\epsilon^2}\int_\Omega \frac{\partial\psi_e(\mathbf{Q}_{h,k})}{\partial\mathbf{Q}} : \mathbf{P}\,d\mathbf{x} + \int_\Omega \frac{\partial\chi(\mathbf{Q}_{h,k})}{\partial\mathbf{Q}} : \mathbf{P}\,d\mathbf{x}, \quad \forall\mathbf{P}\in\mathbb{S}_h(\Omega_h)\cap\mathbb{V}(\mathbf{0}).
\end{aligned} \tag{77}$$

We iterate this procedure until some stopping criteria is achieved. As is the case with the Landau-de Gennes model, solving (77) at each time-step requires Newton's method, i.e. we must compute the gradient and Hessian of the energy. In particular, we need to compute the gradient and Hessian of the singular bulk potential $\psi_c \equiv Tf$, as we detail in Section 5.

5. Evaluating the Singular Bulk Potential

As in other self consistent mean field theories, the main difficulty with the method is that *no explicit formula* for $f(\mathbf{Q})$ is available. Instead, one has to solve the mean field self-consistency equation (37) numerically for a given $\mathbf{Q}$. In the application of Newton's method to the solution of (77), we must compute $\partial\psi_c(\mathbf{Q})/\partial\mathbf{Q}$ and $\partial^2\psi_c(\mathbf{Q})/\partial\mathbf{Q}^2$, evaluated at the current guess of the solution $\mathbf{Q}_{h,k+1}$, where $\psi_c \equiv Tf$. Since $\mathbf{Q}_{h,k+1} = \mathbf{Q}_{h,k+1}(\mathbf{x})$ is spatially varying, this can potentially be very expensive to compute. However, note the presence of the Lagrange interpolation operator $\mathcal{I}_h$ in (77), i.e. see the term $\mathcal{I}_h\left(\partial\psi_c(\mathbf{Q}_{h,k+1})/\partial\mathbf{Q}\right)$. Hence, f, and its derivatives, need only be evaluated at the finite element degrees-of-freedom (or nodes) of the mesh. Moreover, the computation at each node is completely independent of all other nodes, i.e. it is *embarrassingly parallel*. Therefore, the numerical implementation of the singular bulk potential is completely tractable.

There are two main steps involved in the determination of the bulk potential $f(\mathbf{Q})$ and its derivatives: the calculation of the single particle partition function (36), and the solution of the mean field self consistency equation (37). We establish here some of the properties necessary for their calculation.

5.1. Differentiability

We require the gradient and Hessian of $f(\mathbf{Q})$ in solving (77) via Newton's method.

Proposition 7. *Given $\mathbf{Q} \in \mathbf{\Xi}$ with eigenvalues that satisfy $-1/3 < \lambda_i(\mathbf{Q}) < 2/3$, let $\mathbf{A} \in \mathbf{\Xi}$ be the unique minimizer of (49). Then, there holds*

$$\begin{aligned} f(\mathbf{Q}) = \mathbf{Q} : \mathbf{A} - \ln Z(\mathbf{A}) = -W(\mathbf{A}), \\ \frac{\partial f(\mathbf{Q})}{\partial \mathbf{Q}} : \mathbf{P} = \mathbf{A} : \mathbf{P}, \quad \textit{for all } \mathbf{P} \in \mathbf{\Xi}, \\ \mathbf{T} : \frac{\partial^2 f(\mathbf{Q})}{\partial \mathbf{Q}^2} : \mathbf{P} = \left(\frac{\partial \mathbf{A}}{\partial \mathbf{Q}} : \mathbf{T} \right) : \mathbf{P}, \quad \textit{for all } \mathbf{P}, \mathbf{T} \in \mathbf{\Xi}, \end{aligned} \tag{78}$$

where $\partial \mathbf{A}/\partial \mathbf{Q} : \mathbf{T}$ is the unique solution of the linear system

$$\left(\frac{\partial \mathbf{A}}{\partial \mathbf{Q}} : \mathbf{T} \right) : \frac{\partial^2 W(\mathbf{A})}{\partial \mathbf{A}^2} : \mathbf{P} = \mathbf{T} : \mathbf{P}, \quad \textit{for all } \mathbf{P} \in \mathbf{\Xi}, \tag{79}$$

for any $\mathbf{T} \in \mathbf{\Xi}$, where $\partial^2 W(\mathbf{A}) / \partial \mathbf{A}^2$ is the constant 4-tensor evaluated at $\mathbf{A}$.

Proof. Let ρ be the probability distribution given by (36). Then, by (35),

$$\begin{aligned} f(\mathbf{Q}) &= \int_{S^2} \rho(\mathbf{p}) \ln \rho(\mathbf{p}) \, dS(\mathbf{p}) = \int_{S^2} \frac{\exp\left(\mathbf{p}^T \mathbf{A} \mathbf{p}\right)}{Z(\mathbf{A})} \left(\mathbf{p}^T \mathbf{A} \mathbf{p} - \ln Z(\mathbf{A}) \right) dS(\mathbf{p}), \\ &= \mathbf{A} : \int_{S^2} \left(\mathbf{p} \otimes \mathbf{p} - \frac{1}{3} \mathbf{I} \right) \rho(\mathbf{p}) \, dS(\mathbf{p}) - \ln Z(\mathbf{A}) = \mathbf{Q} : \mathbf{A} - \ln Z(\mathbf{A}) = -W(\mathbf{A}), \end{aligned} \tag{80}$$

where we used (8) and (49). Next, using (80),

$$\begin{aligned} \frac{\partial f(\mathbf{Q})}{\partial \mathbf{Q}} : \mathbf{P} &= \mathbf{P} : \mathbf{A} + \mathbf{Q} : \mathbf{A}' - \frac{1}{Z(\mathbf{A})} \frac{\partial Z(\mathbf{A})}{\partial \mathbf{A}} : \mathbf{A}' = \mathbf{P} : \mathbf{A} + \mathbf{Q} : \mathbf{A}' - \left(\mathbf{Q} + \frac{1}{3} \mathbf{I} \right) : \mathbf{A}' \\ &= \mathbf{P} : \mathbf{A} + \mathbf{Q} : \mathbf{A}' - \mathbf{Q} : \mathbf{A}' = \mathbf{A} : \mathbf{P}, \end{aligned} \tag{81}$$

where $\mathbf{\Xi} \ni \mathbf{A}' \equiv (\partial \mathbf{A}/\partial \mathbf{Q}) : \mathbf{P}$ and we used (47).

By differentiating (81), we clearly get the last line of (78). Thus, we need a characterization of $\partial \mathbf{A}/\partial \mathbf{Q}$. Recall that $\mathbf{A}$ is the unique minimizer of (49), i.e. $\mathbf{A}$ satisfies (54). So, we differentiate (54) with respect to $\mathbf{Q}$, in the direction $\mathbf{T}$:

$$\left(\frac{\partial \mathbf{A}}{\partial \mathbf{Q}} : \mathbf{T} \right) : \frac{\partial^2 W(\mathbf{A})}{\partial \mathbf{A}^2} : \mathbf{P} = \mathbf{T} : \mathbf{P}, \quad \text{for all } \mathbf{P} \in \mathbf{\Xi}. \tag{82}$$

□

Remark 8. *The 4-tensor $\partial^2 W(\mathbf{A}) / \partial \mathbf{A}^2$ is positive definite, but the coercivity constant degrades as $|\mathbf{A}| \to \infty$.*

5.2. Optimization Procedure

Given $\mathbf{Q}$, we describe a procedure to obtain the corresponding $\mathbf{A} = \mathbf{A}(\mathbf{Q})$, as well as its derivative with respect to $\mathbf{Q}$.

5.2.1. Solving the Euler-Lagrange Equation

Recall (49) and define the linear form $F_{\mathbf{Q}}(\mathbf{A};\mathbf{P})$ to be the first variation of (49) with respect to $\mathbf{A}$:

$$F_{\mathbf{Q}}(\mathbf{A};\mathbf{P}) := \frac{1}{Z(\mathbf{A})}\frac{\partial Z(\mathbf{A})}{\partial \mathbf{A}} \cdot \mathbf{P} - \mathbf{Q} : \mathbf{P}. \tag{83}$$

Thus, given $\mathbf{Q} \in \boldsymbol{\Xi}$, we want to find $\mathbf{A}$ such that $F_{\mathbf{Q}}(\mathbf{A};\mathbf{P}) = 0$ for all $\mathbf{P} \in \boldsymbol{\Xi}$. In other words, we want to find a zero of the non-linear function $F_{\mathbf{Q}}(\cdot;\mathbf{P})$. Hence, we apply Newton's method.

For a given $\mathbf{A}$, define the bilinear form:

$$\begin{aligned} m_{\mathbf{A}}(\mathbf{P},\mathbf{T}) &:= \frac{\partial}{\partial \mathbf{A}} F_{\mathbf{Q}}(\mathbf{A};\mathbf{P}) : \mathbf{T} \\ &= \frac{1}{Z(\mathbf{A})}\mathbf{P} : \frac{\partial^2 Z(\mathbf{A})}{\partial \mathbf{A}^2} : \mathbf{T} - \frac{1}{Z(\mathbf{A})}\left(\frac{\partial Z(\mathbf{A})}{\partial \mathbf{A}} : \mathbf{P}\right)\frac{1}{Z(\mathbf{A})}\left(\frac{\partial Z(\mathbf{A})}{\partial \mathbf{A}} : \mathbf{T}\right). \end{aligned} \tag{84}$$

Then Newton's method is as follows.

- Initialize. Set $\mathbf{A}_0 \in \boldsymbol{\Xi}$ (can take the zero 3×3 matrix) and set $k = 0$.
- While not converged, do:
  1. Solve the following (linear) variational problem. Find $\delta\mathbf{A}_{k+1} \in \boldsymbol{\Xi}$ such that
  $$m_{\mathbf{A}_k}(\delta\mathbf{A}_{k+1},\mathbf{P}) = -F_{\mathbf{Q}}(\mathbf{A}_k;\mathbf{P}), \quad \forall \mathbf{P} \in \boldsymbol{\Xi}. \tag{85}$$
  2. Update. Set $\mathbf{A}_{k+1} := \mathbf{A}_k + \delta\mathbf{A}_{k+1}$.
  3. If $|\delta\mathbf{A}_{k+1}|$ is less than some tolerance, then stop.
  4. Else, set $k \leftarrow k+1$ and return to Step (1).

Let $\mathbf{A}_*$ be the solution, i.e. $F_{\mathbf{Q}}(\mathbf{A}_*;\mathbf{P}) = 0$ for all $\mathbf{P} \in \boldsymbol{\Xi}$. Let $\mathbf{A}'_*(\mathbf{T}) = (\partial\mathbf{A}/\partial\mathbf{Q}) : \mathbf{T}$. We obtain $\mathbf{A}'_*(\mathbf{T})$ as the unique solution of the following variational problem. Find $\mathbf{A}'_*(\mathbf{T}) \in \boldsymbol{\Xi}$, for every $\mathbf{T} \in \boldsymbol{\Xi}$, such that

$$m_{\mathbf{A}_*}(\mathbf{A}'_*(\mathbf{T}),\mathbf{P}) = \mathbf{T} : \mathbf{P}, \quad \forall \mathbf{P} \in \boldsymbol{\Xi}. \tag{86}$$

5.2.2. Matrix-Vector Form

Recall the basis $\{\mathbf{E}^k\}_{k=1}^5$ that spans $\boldsymbol{\Xi}$. We rewrite the Newton method in terms of this basis.

- Initialize. Let $\boldsymbol{\alpha}_0 \in \mathbb{R}^5$, with $\boldsymbol{\alpha}_0 = (\alpha_0^1, ..., \alpha_0^5)$, such that $\mathbf{A}_0 = \sum_{\ell=1}^5 \alpha_0^\ell \mathbf{E}^\ell$. Can simply take $\boldsymbol{\alpha}_0 = \mathbf{0}$. Set $k = 0$.
- While not converged, do:

1. Compute. Let $\mathbf{b}_k \in \mathbb{R}^5$ such that $b_k^\ell = -F_{\mathbf{Q}}(\mathbf{A}_k; \mathbf{E}^\ell)$ for $\ell = 1, ..., 5$. Moreover, let $\mathbf{H}_k \in \mathbb{R}^{5\times 5}$, i.e. $\mathbf{H}_k = [h_k^{ij}]_{i,j=1}^5$, such that $h_k^{ij} = m_{\mathbf{A}_k}(\mathbf{E}^i, \mathbf{E}^j)$ for $1 \le i, j \le 5$.
2. Solve for $\delta\boldsymbol{\alpha}_{k+1} \in \mathbb{R}^5$:

$$\mathbf{H}_k(\delta\boldsymbol{\alpha}_{k+1}) = \mathbf{b}_k \tag{87}$$

3. Update. Set $\boldsymbol{\alpha}_{k+1} := \boldsymbol{\alpha}_k + \delta\boldsymbol{\alpha}_{k+1}$, and define $\mathbf{A}_{k+1} = \sum_{\ell=1}^5 \alpha_{k+1}^\ell \mathbf{E}^\ell$.
4. If $|\delta\boldsymbol{\alpha}_{k+1}|$ is less than some tolerance, then stop.
5. Else, set $k \leftarrow k + 1$ and return to Step (1).

Let $\mathbf{A}_*$ be the solution, i.e. $F_{\mathbf{Q}}(\mathbf{A}_*; \mathbf{P}) = 0$ for all $\mathbf{P} \in \boldsymbol{\Xi}$. Let $\mathbf{A}'_*(\mathbf{E}^\ell) = (\partial\mathbf{A}/\partial\mathbf{Q}) : \mathbf{E}^\ell$, for each $\ell = 1, ..., 5$, and let $(\boldsymbol{\alpha}'_*)^\ell \in \mathbb{R}^5$ be such that

$$\mathbf{A}'_*(\mathbf{E}^\ell) = \sum_{k=1}^5 [(\boldsymbol{\alpha}'_*)^\ell \cdot \mathbf{e}_k]\mathbf{E}^k. \tag{88}$$

Next, let $\mathbf{H}_*$ be the Hessian matrix corresponding to $\mathbf{A}_*$. Then, we obtain $\mathbf{A}'_*(\mathbf{E}^\ell)$ by solving for $(\boldsymbol{\alpha}'_*)^\ell$ the equation

$$\mathbf{H}_*(\boldsymbol{\alpha}'_*)^\ell = \mathbf{e}_\ell, \quad \text{for each } \ell = 1, ..., 5. \tag{89}$$

Note: this is a one time solve (there is no Newton iteration).

5.2.3. Computational Issues

The main difficulty associated with our method is that, contrary to the case of the Landau-de Gennes energy (or the Oseen-Frank energy in the director representation of the nematic), the energy density as a function of $\mathbf{Q}$ is not known explicitly. As in other self consistent field theories, practical computation requires a numerical scheme. In this case, the approximation involved in the evalulation of the free energy of a configuration is due to both the Lagrange interpolation operator $\mathcal{I}_h$ in (77), and the fact that integrals on the unit sphere *cannot be computed exactly.* Hence we must address the following issues.

- The integrals must be approximated by quadrature, ideally a high order quadrature rule.
- The strict convexity of the functional in (49) degrades as $|\mathbf{A}|$ becomes large, and this is exactly the situation that arises when the eigenvalues of $\mathbf{Q}$ approach the physical limits in (10). Thus, any inaccuracies in the computations (e.g. the integrals) can adversely affect the convergence of the Newton method.
- Furthermore, when $\mathbf{A}$ becomes large, $\exp\left(\mathbf{p}^T\mathbf{A}\mathbf{p}\right)$ becomes extremely large. Even though we divide by $Z(\mathbf{A})$, there could be an intermediate overflow result or inaccuracies.

Therefore, we introduce the following modifications of the optimization method described earlier. Before computing any of the above, first do an eigen-decomposition of $\mathbf{Q}$. If the eigenvalues are in the range:

$$-\frac{1}{3} + \delta_0 \leq \lambda_i(\mathbf{Q}) \leq \frac{2}{3} - \delta_0, \quad \text{for } i = 1, 2, 3, \tag{90}$$

for some $\delta_0 > 0$, then the plain Newton method above is sufficient (it converges in ≈ 5 iterations). Numerical experience indicates that $\delta_0 = 0.05$ to 0.1 is adequate. If the eigenvalues are outside the range (90), then one must use a sufficiently accurate quadrature rule to ensure that the system in (83) is accurately approximated. In addition, a more robust optimization procedure should be used (e.g., the Broyden-Fletcher-Goldfarb-Shanno algorithm with a line search to ensure the objective function decreases) to account for possible numerical sensitivities. This is not difficult to implement since the problem size is small. However, we have not explored this possibility yet.

Next, as a general concern, the integrals should be computed using a shifting procedure. For example, consider the computation of

$$\frac{1}{Z(\mathbf{A})}\frac{\partial Z(\mathbf{A})}{\partial \mathbf{A}} = \frac{1}{\int_{S^2} \exp\left(\mathbf{p}^T\mathbf{A}\mathbf{p}\right)\, dS(\mathbf{p})} \int_{S^2} (\mathbf{p}\otimes\mathbf{p}) \exp\left(\mathbf{p}^T\mathbf{A}\mathbf{p}\right)\, dS(\mathbf{p}), \tag{91}$$

for a given $\mathbf{A} \in \boldsymbol{\Xi}$. Let $C_0 = |\mathbf{A}|$. Then, (91) is equivalent to

$$\frac{1}{Z(\mathbf{A})}\frac{\partial Z(\mathbf{A})}{\partial \mathbf{A}} = \frac{1}{\int_{S^2} \exp\left(\mathbf{p}^T\mathbf{A}\mathbf{p} - C_0\right)\, dS(\mathbf{p})} \int_{S^2} (\mathbf{p}\otimes\mathbf{p}) \exp\left(\mathbf{p}^T\mathbf{A}\mathbf{p} - C_0\right)\, dS(\mathbf{p}). \tag{92}$$

The advantage of (92) over (91) is that, when $|\mathbf{A}|$ is large, (92) will *not* result in an overflow calculation.

Lastly, all the integrals over the unit sphere have been approximated by Lebedev quadrature [63]. We ascertain the accuracy of the computation in section 6.1. However, we note that they involve uniformly distributed points, so when the probability distribution ρ becomes very localized, the integration may fail. We have not encountered this problem in our numerical results below, but note that it would be possible to use an adaptive quadrature method instead. Indeed, one could adapt the quadrature rule depending on the performance of the Newton solve, or on how close the eigenvalues are to the physical limits.

6. Results

All simulations were implemented using the Matlab/C++ finite element toolbox FELICITY [64, 65]. For all 3-D simulations, we used the algebraic multigrid solver (AGMG) [66, 67, 68, 69] to solve the linear systems appearing in Newton's method. In 2-D, we simply used the "backslash" command in Matlab. Numerical calculations were performed with Matlab version R2017b on a Haswell processor with a base clock of 2.5 Ghz at the Minnesota Supercomputing Institute. Spatially distributed Newton iterations were paralleized over

Table 1: Maximum component of the difference $\mathbf{A}_{max} - \mathbf{A}$, for $\mathbf{A}$ given by Newton's method for various Lebedev quadrature degrees and $\mathbf{Q}$ with various eigenvalues parametrized by S_n. $\mathbf{A}_{max}$ is given by Newton's method with maximum quadrature degree 5810.

Degree	$S_n = 0.1$	$S_n = 0.6$	$S_n = 0.97$	$S_n = 0.995$
14	0.04	1.4	49.6	No Convergence
86	3.2×10^{-9}	1.4×10^{-3}	31.2	No Convergence
590	1.8×10^{-15}	6.8×10^{-14}	7.1×10^{-3}	No Convergence
2030	7.2×10^{-15}	5.1×10^{-14}	5.1×10^{-12}	0.1
3470	2.3×10^{-14}	6.6×10^{-14}	1.9×10^{-12}	3.3×10^{-4}
$\lvert\mathbf{A}_{max}\rvert$	0.82	5.1	58.3	347

24 threads (Matlab `parfor`). Execution timings given below correspond to this configuration.

In our simulations, we chose $\epsilon = 1$. We also tested the method with smaller values of ϵ, and a finer mesh, and there were no issues. The number of iterations needed to relax increased roughly proportional to the decrease in ϵ^2. But the end result was the same.

6.1. Accuracy of Newton's Method

We first look at the accuracy of Newton's method described in Sec. 5.2 to invert the mean field self consistency relation, and obtain the Lagrange multiplier $\mathbf{A}(\mathbf{Q})$. To test this, we run the procedure for various degrees of the Lebedev quadrature. We use in the test a tensor $\mathbf{Q}$ with maximum eigenvalue parametrized as $\max_i(\lambda_i) = (2/3)S_n$, for a range of S_n. We have examined the cases $S_n = 0.1$, $S_n = 0.6$, $S_n = 0.97$, and $S_n = 0.995$, which is the largest value of S_n for which the algorithm converges. Note that if $S_n = -0.5$ or 1, the physical limit of the eigenvalues is reached, $\mathbf{Q}$ is no longer physical, and the corresponding $\mathbf{A}$ diverges. The maximum degree of the Lebedev quadrature tested is 5810, and we denote $\mathbf{A}$ given by quadrature at this degree by $\mathbf{A}_{max}$. Table 1 summarizes the results in terms of the maximum component of the difference $\mathbf{A}_{max} - \mathbf{A}$ for various quadrature degrees. We find that for quadrature degrees below 500, the eigenvalues of $\mathbf{Q}$ must be relatively small in order to obtain accurate values of $\mathbf{A}$. For $\mathbf{Q}$ with eigenvalues close to the their physical limit, the Lebedev quadrature degree must be sufficiently high. Depending on the value of κ/T, it may be necessary to use larger degrees of quadrature or more sophisticated methods to find $\mathbf{A}$, as illustrated in Figure 2 showing the bulk potential, Eq. (18), as a function of S_n. As κ/T increases, and the liquid crystal becomes more ordered, the equilibrium value of S_n increases.

6.2. Boundedness of the bulk potential

We next examine two spatially nonuniform configurations which are unstable in the Landau-de Gennes theory when $L_* \neq 0$, but remain stable when using the singular bulk potential. In the first example, we choose a weakly perturbed configuration away from uniform. We take as initial condition a purely uniaxial

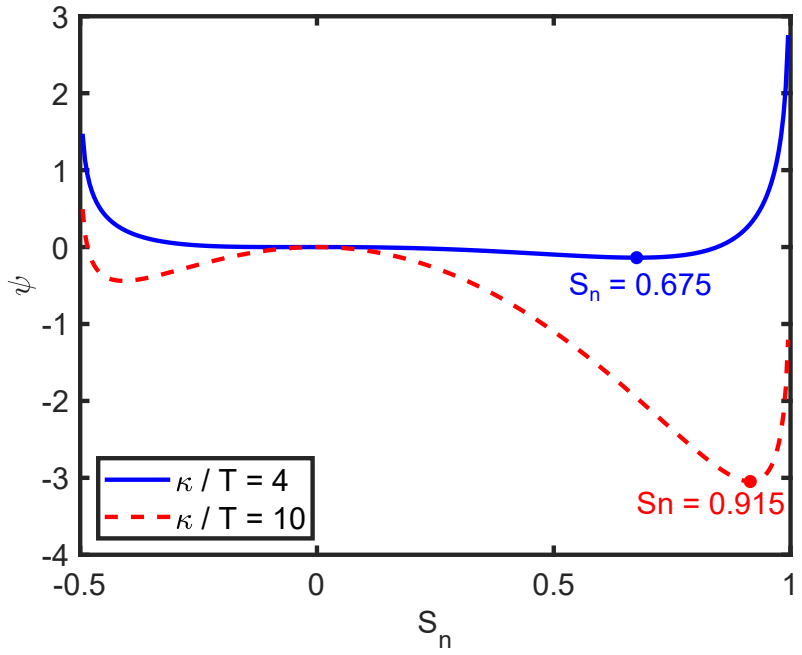

Figure 2: Singular bulk potential, Eq. (18), as a function of S_n for $\kappa/T = 4$ and $\kappa/T = 10$. Dots show the location of the minimum for either case. As κ/T increases, the minimum of the bulk potential approaches the physical limit of $S_n = 1$.

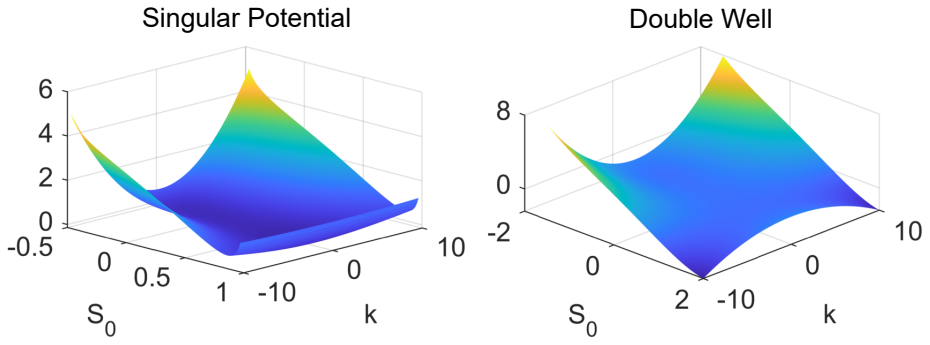

Figure 3: Energy of the perturbed uniform configuration as a function of S_0 and k for the Maier-Saupe bulk potential and the double well potential when $L_1 = 1$, $L_2 = L_3 = L_4 = 0$ $L_* = 3$. In the case of the double well, there is a saddle point and unbounded energy, while the Maier-Saupe energy remains bounded below since it diverges if $S \to -0.5$ or $S \to 1$.

configuration defined by $\mathbf{Q} = S_n(x)(\hat{\mathbf{n}} \otimes \hat{\mathbf{n}} - 1/3\mathbf{I})$ where $\mathbf{I}$ is the identity matrix, $\hat{\mathbf{n}} = (0, 1, 0)$ is fixed, and $S_n(x) = S_0 + \beta \sin \pi k x$, where $S_0 = 0.6751$ is chosen so as to minimize the bulk potential with $\kappa/T = 4$. We set $\beta = 0.1$, $k = 10$, $L_1 = 1$, $L_2 = L_3 = L_4 = 0$, and $L_* = 3$. For this ratio of κ/T, the equilibrium configuration is inside the nematic phase. Note that the coefficients are just outside the limits stated in Theorem 5, but the minimizer found appears to be robust.

We run the gradient flow described in Sec. 4.2 on the components of $\mathbf{Q}$, decomposed in the basis

$$\mathbf{E}_1 = \begin{pmatrix} \frac{2}{\sqrt{3}} & 0 & 0 \\ 0 & -\frac{1}{\sqrt{3}} & 0 \\ 0 & 0 & -\frac{1}{\sqrt{3}} \end{pmatrix}, \quad \mathbf{E}_2 = \begin{pmatrix} 0 & 0 & 0 \\ 0 & 1 & 0 \\ 0 & 0 & -1 \end{pmatrix}, \quad \mathbf{E}_3 = \begin{pmatrix} 0 & 1 & 0 \\ 1 & 0 & 0 \\ 0 & 0 & 0 \end{pmatrix}, \quad \mathbf{E}_4 = \begin{pmatrix} 0 & 0 & 1 \\ 0 & 0 & 0 \\ 1 & 0 & 0 \end{pmatrix}, \quad \mathbf{E}_5 = \begin{pmatrix} 0 & 0 & 0 \\ 0 & 0 & 1 \\ 0 & 1 & 0 \end{pmatrix}, \tag{93}$$

using a square domain defined by $[0, 1]^2$ with a body centered mesh with 150×150 squares (44701 vertices), linear basis functions, and a time step in the minimization $\delta t = 4 \times 10^{-3}$. The same parameters are used for both the singular bulk potential and the standard bulk potential of Landau-de Gennes (see (7)). When $L_* \neq 0$, the total LdG energy with standard double well potential is unbounded from below when $k > 0$. However, the singular bulk potential maintains a bounded free energy for a nonzero range of L_* since it diverges outside of the range $-1/2 \leq S_n \leq 1$. This is illustrated in Fig. 3 where we show the total free energy for a set of configurations within a range of S_0 and k. The (standard) double well energy has a saddle along the line $k = 0$ indicating lack of stability for any k and a range of amplitudes S_0. On the other hand, given the divergence of the Maier-Saupe bulk potential outside the admissible range

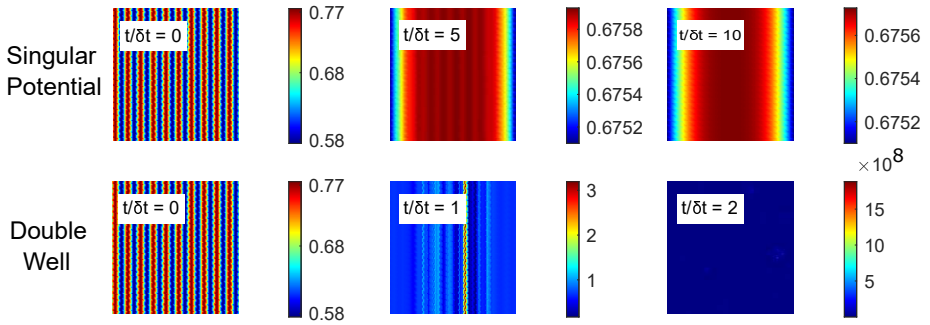

Figure 4: Comparison of the evolution of S_n for the perturbed uniform configuration given by Maier-Saupe bulk potential, and that given by the Landau-de Gennes double well potential. We use $k = 10$, $\beta = 0.1$, and $L_* = 3$. The evolution corresponding to the Maier-Saupe bulk potential relaxes to a uniform configuration, while the configuration evolving under the double well diverges rapidly.

of eigenvalues of $\mathbf{Q}$, the free energy computed remains bounded below for all admissible values of S_0 and k. In fact, the surface plot.

To further illustrate the difference between the two energies, we show in Fig. 4 the gradient flow of S_n during the minimization procedure described in Sec. 4.2. The configuration obtained by iterating with the standard Landau-de Gennes double well energy diverges quickly, whereas in the Maier-Saupe case, it simply relaxes to a uniform configuration.

The second configuration studied is an adaptation of the example from Ball and Majumdar [31] meant to demonstrate the stability of the singular bulk potential. We consider a cylindrically symmetric initial condition $\mathbf{Q} = S_n(r)(\hat{\mathbf{r}} \otimes \hat{\mathbf{r}} - 1/3\mathbf{I})$ with

$$S_n(r) = \begin{cases} S_0(2 + \sin \frac{\pi k r}{5}) & 0 < r < 5 \\ 2S_0(2 + \sin \pi k)(1 - \frac{r}{10}) & 5 < r < 10. \end{cases} \tag{94}$$

This initial condition is allowed to relax by gradient flow as in Sec. 4.2. The value of $S_0 = 0.32$ is chosen so that the eigenvalues of $\mathbf{Q}$ are close to the physically admissible limit, and $\kappa/T = 3$ so that the bulk potential is minimized for the isotropic phase $S = 0$ [42]. We also set $k = 5$, $L_1 = 1$, $L_2 = L_3 = L_4 = 0$, and $L_* = 3$. A body centered mesh with 150×150 squares in a square domain with bounds $[-10, 10]^2$, and time step $\delta t = 4 \times 10^{-3}$ are used. Each iteration of the gradient flow for this mesh size takes ~ 30 CPU minutes to complete. By direct substitution of Eq. (94) into the Landau-de Gennes free energy, Ball and Majumdar showed that the energy is unbounded below if there is no constraint on the value of S_0 when $L_* \neq 0$ [31]. Figure 5 shows several time steps in the in the gradient flow of S_n for the initial condition (94) with both the singular bulk potential and the standard double well Landau-de Gennes potential. As expected, the flow corresponding to the standard double well potential fails to

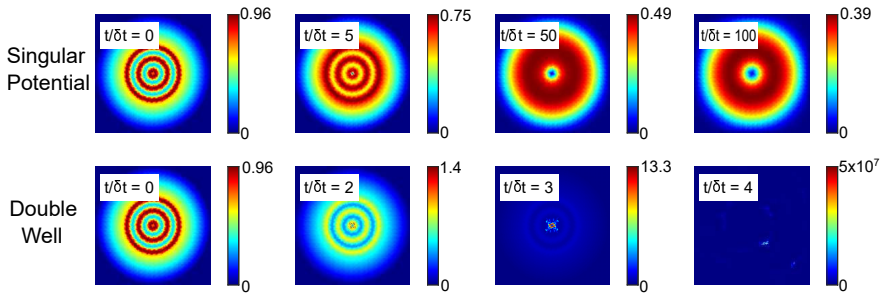

Figure 5: Evolution of S_n for the example from Ball and Majumdar [31] for the Maier-Saupe bulk potential and standard bulk potential with $k = 5$ and $L_* = 3$. The system with the Maier-Saupe potential eventually relaxes to the isotropic phase, while the double well system diverges rapidly.

converge when $L_* \neq 0$, whereas the singular bulk potential eventually converges to a configuration with uniform eigenvalues.

6.3. Three dimensional configurations

Although the self consistent field theoretic method introduced might appear to lead to a more complex numerical implementation than the Landau-de Gennes theory, we show that even with modest computational resources it is possible to obtain defected configurations in three spatial dimensions. We consider three examples: a $m = +1$ point defect, a line disclination of charge $m = -1/2$, and a Saturn ring loop disclination. For all calculations we use $\kappa/T = 4$, $L_1 = 1$, $L_2 = L_3 = L_4 = 0$, and $L_* = 3$. As above, the equilibrium configuration is in the nematic phase. For the point defect and line disclination, we use a cubic domain with bounds $[-5, 5]^3$ with a uniform tetrahedral mesh with $41 \times 41 \times 41$ vertices. For the Saturn ring we use a cubic domain of size $[-30, 30]^3$ with a spherical cavity of radius 7.5 and a body-centered-cubic (bcc) mesh with 127108 vertices. For all computations, we use piecewise linear finite elements and a time step $\delta t = 5 \times 10^{-2}$. Iteration is continued until the energy change falls within a tolerance of 10^{-6}. For the point defect, Dirichlet boundary conditions on the components of $\mathbf{Q}$ are used on all sides of the computational domain so as to enforce the topological charge of the defect at the center. For the line disclination, Neumann boundary conditions on the components of $\mathbf{Q}$ are used on the top and bottom of the computational domain, while Dirichlet conditions are used on all lateral sides to maintain the topological charge of the line at the center of the domain. For the Saturn ring, Dirichlet boundary conditions fixing a uniform configuration with molecules oriented along the z-axis are used on the exterior sides of the domain while Dirichlet conditions are used on the interior sphere to fix a configuration with molecules oriented radially.

Figure 6 shows 3D visualizations of equilibrium configurations for a $m = +1$ point defect and a $m = -1/2$ line disclination. Both simulations reach equilibrium in $\sim$ 12 CPU hours. The surfaces in both figures show all points

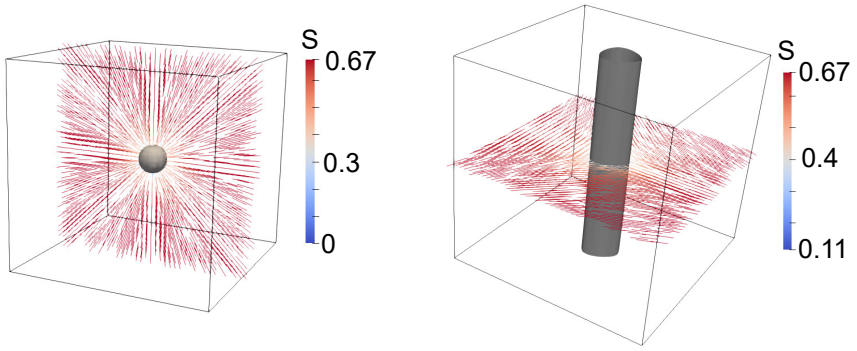

Figure 6: 3D visualization of the equilibrium configurations for a $m = +1$ point defect (left) and a $m = -1/2$ line disclination (right). For both figures, the surface shows all points where $S_n = 0.5S_{max}$ i.e. the "boundaries" of the defects. For both simulations we set $\kappa/T = 4$, $L_1 = 1$, $L_2 = L_3 = L_4 = 0$ and $L_* = 3$.

where $S_n = 0.5S_{max}$ which we define as the "boundary" of the defect. Note that for the line disclination, the eigenvalue profile is not isotropic due to the inclusion of cubic order terms in the elastic free energy. Also note that the defect core becomes biaxial, that is, the eigenvalues of $\mathbf{Q}$ become distinct. These two features are shown clearly in Figure 7, which shows a cut in $z = 0$ plane of S_n along with the molecular orientation probability distribution, $\rho(\mathbf{p})$, at various points through the defect. Far from the defect, the distribution is uniaxial and the corresponding $\mathbf{Q}$ has two degenerate eigenvalues. As the core of the defect is approached, the distribution spreads out in the xy plane and the corresponding $\mathbf{Q}$ has three distinct eigenvalues. At the center of the defect, the distribution is once again uniaxial but now corresponds to a disk with all orientations in the xy plane equally weighted, which is distinct from the commonly referred to phenomenon of "escape to the third dimension" [1]. This biaxiality and the anisotropy is consistent with experimental observations in chromonic lyotropic liquid crystals [70], and has been discussed in detail in [43].

Finally, Figure 8 shows a 3D visualization and a cut through the $x = 0$ plane of a Saturn ring loop disclination around a particle with homeotropic anchoring. As before, the surface shows all points on the "boundary" of the defect while the cut shows the value of S_n. The shape of the defect and the director field with a characteristic $m = -1/2$ charge are consistent with previous investigations of the Saturn ring [71, 72]. The Saturn ring configuration takes ~ 84 CPU hours to reach equilibrium. This is longer than the other 3D simulations because the mesh is larger and the system requires more iterations to reach equilibrium.

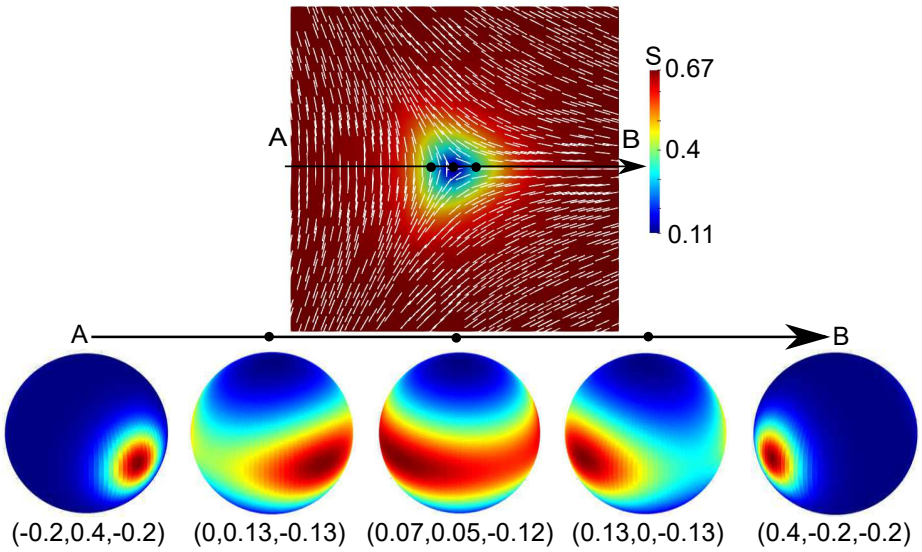

Figure 7: Cut of the equilibrium configuration of S_n in the $z = 0$ plane for a disclination line with plots of the molecular orientation probability distribution, $\rho(\mathbf{p})$, at various points through the disclination. The distribution becomes biaxial as the core of the defect is approached. At the center of the core all orientations in the xy plane are equally probable. The eigenvalues of $\mathbf{Q}$ are listed below the corresponding distribution as $(\lambda_1, \lambda_2, \lambda_3)$.

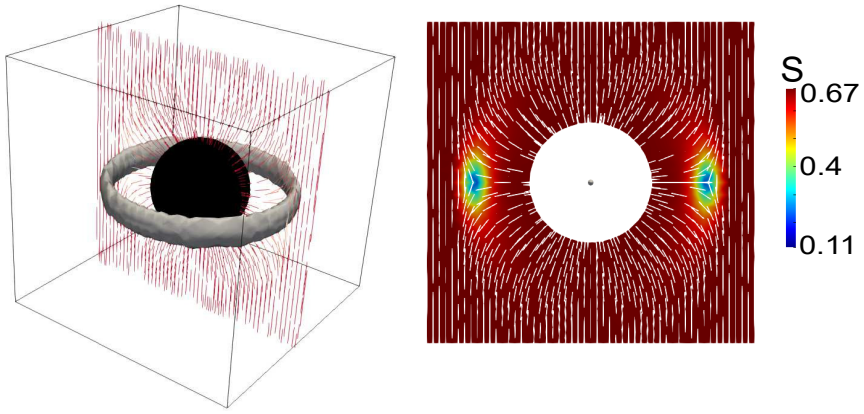

Figure 8: 3D visualization of the equilibrium configuration for a Saturn ring loop disclination (left) and plot of S_n in the $x = 0$ plane for the same configuration (right). The surface shows all points where $S_n = 0.5 S_{max}$ i.e. the "boundary" of the defect. For the simulation we set $\kappa/T = 4$, $L_1 = 1$, $L_2 = L_3 = L_4 = 0$ and $L_* = 3$.

7. Conclusions and discussion

The analysis of a new computational method to obtain equilibrium configurations of a nematic liquid crystal has been presented. The method, based on the Ball-Majumdar singular bulk potential, can overcome known limitations of the Landau-de Gennes theory in the case of elastically anisotropic media. We present selected numerical results demonstrating the convergence of the method in cases in which the Landau-de Gennes theory fails, and a study of prototypical three dimensional configurations that include both point and line topological defects. The code developed has been incorporated into the FELICITY finite element framework in order to facilitate adoption [64, 65].

The results shown have been obtained with a particular microscopic interaction model: the Maier-Saupe contact potential. This is a simple case to study since the resulting interaction energy is simply quadratic in $\mathbf{Q}$. However, the extension to more complex interaction energies is possible assuming one knows their explicit functional representation in terms of the mesoscale $\mathbf{Q}$. The eigenvalue constraint as introduced is captured in the entropy functional, which only depends on the definition of $\mathbf{Q}$, and hence is independent of the form of the interaction energy functional. Of course, the limitation of a mean field approximation remains as long as the energy only depends on the local statistical average of the molecular orientation $\mathbf{p}$. This is not expected to be a serious shortcoming as long as thermal fluctuations are negligible. This is the case in the majority of contemporary studies that focus on systems deep inside the nematic phase.

We have restricted our analysis to finding minimizers of the free energy functional, but the method can be readily extended to studies of nematodynamics (including hydrodynamic interactions). One simply needs to replace the Landau-de Gennes functional by the free energy computed from the singular potential. While there is an additional computational cost involved, it is not severe as demonstrated by our calculations of defect configurations in three dimensions, as long as one takes advantage of parallelism. The method can be therefore applied to the study of the temporal evolution of elastically anisotropic systems, including mass flows. Such a capability should be specially relevant to studies of nematic active matter in which the length of the molecular constituents, and the dependence of their elastic constants on the Debye length when charged, leads to strong elastic anisotropy.

References

[1] P. G. de Gennes, J. Prost, The Physics of Liquid Crystals, 2nd Edition, Vol. 83 of International Series of Monographs on Physics, Oxford Science Publication, Oxford, UK, 1995.

[2] J. P. Lagerwall, G. Scalia, A new era for liquid crystal research: Applications of liquid crystals in soft matter nano-, bio- and microtechnology, Current Applied Physics 12 (6) (2012) 1387 – 1412.

doi:https://doi.org/10.1016/j.cap.2012.03.019.
URL http://www.sciencedirect.com/science/article/pii/S1567173912001113

[3] L. Blinov, Electro-optical and magneto-optical properties of liquid crystals, Wiley, 1983.

[4] J. W. Goodby, Handbook of Visual Display Technology (Editors: Chen, Janglin, Cranton, Wayne, Fihn, Mark), Springer, 2012, Ch. Introduction to Defect Textures in Liquid Crystals, pp. 1290–1314.

[5] J. Sun, H. Wang, L. Wang, H. Cao, H. Xie, X. Luo, J. Xiao, H. Ding, Z. Yang, H. Yang, Preparation and thermo-optical characteristics of a smart polymer-stabilized liquid crystal thin film based on smectic A-chiral nematic phase transition, Smart Materials and Structures 23 (12) (2014) 125038.
URL http://stacks.iop.org/0964-1726/23/i=12/a=125038

[6] J. Hoogboom, J. A. Elemans, A. E. Rowan, T. H. Rasing, R. J. Nolte, The development of self-assembled liquid crystal display alignment layers, Philosophical Transactions of the Royal Society of London A: Mathematical, Physical and Engineering Sciences 365 (1855) (2007) 1553–1576. doi:10.1098/rsta.2007.2031.

[7] P. Dasgupta, M. K. Das, B. Das, Fast switching negative dielectric anisotropic multicomponent mixtures for vertically aligned liquid crystal displays, Materials Research Express 2 (4) (2015) 045015.
URL http://stacks.iop.org/2053-1591/2/i=4/a=045015

[8] F. Brochard, L. Léger, R. B. Meyer, Freedericksz transition of a homeotropic nematic liquid crystal in rotating magnetic fields, J. Phys. Colloques 36 (C1) (1975) C1–209–C1–213. doi:10.1051/jphyscol:1975139.

[9] Ágnes Buka, N. Éber (Eds.), Flexoelectricity in Liquid Crystals: Theory, Experiments and Applications, World Scientific, 2012.

[10] A. A. Shah, H. Kang, K. L. Kohlstedt, K. H. Ahn, S. C. Glotzer, C. W. Monroe, M. J. Solomon, Self-assembly: Liquid crystal order in colloidal suspensions of spheroidal particles by direct current electric field assembly (small 10/2012), Small 8 (10) (2012) 1551–1562. doi:10.1002/smll.201290056.

[11] W. Zhu, M. Shelley, P. Palffy-Muhoray, Modeling and simulation of liquid-crystal elastomers, Phys. Rev. E 83 (2011) 051703. doi:10.1103/PhysRevE.83.051703.

[12] W. H. de Jeu (Ed.), Liquid Crystal Elastomers: Materials and Applications, Advances in Polymer Science, Springer, 2012.

[13] J. Biggins, M. Warner, K. Bhattacharya, Elasticity of polydomain liquid crystal elastomers, Journal of the Mechanics and Physics of Solids 60 (4) (2012) 573 – 590. doi:10.1016/j.jmps.2012.01.008.
URL http://www.sciencedirect.com/science/article/pii/S0022509612000166

[14] A. Rešetič, J. Milavec, B. Zupančič, V. Domenici, B. Zalar, Polymer-dispersed liquid crystal elastomers, Nature Communications 7 (2016) 13140. doi:10.1038/ncomms13140.

[15] J. Heo, J.-W. Huh, T.-H. Yoon, Fast-switching initially-transparent liquid crystal light shutter with crossed patterned electrodes, AIP Advances 5 (4) (2015) –. doi:10.1063/1.4918277.

[16] M. Humar, I. Muševič, 3d microlasers from self-assembled cholesteric liquid-crystal microdroplets, Opt. Express 18 (26) (2010) 26995–27003. doi:10.1364/OE.18.026995.
URL http://www.opticsexpress.org/abstract.cfm?URI=oe-18-26-26995

[17] H. Coles, S. Morris, Liquid-crystal lasers, Nature Photonics 4 (10) (2010) 676–685.

[18] M. Camacho-Lopez, H. Finkelmann, P. Palffy-Muhoray, M. Shelley, Fast liquid-crystal elastomer swims into the dark, Nature Materials 3 (5) (2004) 307–310.

[19] T. H. Ware, M. E. McConney, J. J. Wie, V. P. Tondiglia, T. J. White, Voxelated liquid crystal elastomers, Science 347 (6225) (2015) 982–984. arXiv:http://www.sciencemag.org/content/347/6225/982.full.pdf, doi:10.1126/science.1261019.
URL http://www.sciencemag.org/content/347/6225/982.abstract

[20] I. Muševič, S. Žumer, Liquid crystals: Maximizing memory, Nature Materials 10 (4) (2011) 266–268.

[21] T. Lopez-Leon, A. Fernandez-Nieves, Drops and shells of liquid crystal, Colloid and Polymer Science 289 (4) (2011) 345–359. doi:10.1007/s00396-010-2367-7.

[22] S. Čopar, U. Tkalec, I. Muševič, S. Žumer, Knot theory realizations in nematic colloids, Proceedings of the National Academy of Sciences 112 (6) (2015) 1675–1680. arXiv:http://www.pnas.org/content/112/6/1675.full.pdf, doi:10.1073/pnas.1417178112.
URL http://www.pnas.org/content/112/6/1675.abstract

[23] J. K. Whitmer, X. Wang, F. Mondiot, D. S. Miller, N. L. Abbott, J. J. de Pablo, Nematic-field-driven positioning of particles in liquid crystal droplets, Phys. Rev. Lett. 111 (2013) 227801. doi:10.1103/PhysRevLett.111.227801.

[24] M. Wang, L. He, S. Zorba, Y. Yin, Magnetically actuated liquid crystals, Nano Letters 14 (7) (2014) 3966–3971, pMID: 24914876. arXiv:http://dx.doi.org/10.1021/nl501302s, doi:10.1021/nl501302s.
URL http://dx.doi.org/10.1021/nl501302s

[25] S. Shankar, M. C. Marchetti, Hydrodynamics of active defects: from order to chaos to defect ordering, Phys. Rev. X 9 (4) (2019) 041047.

[26] S. Shankar, A. Souslov, M. J. Bowick, M. C. Marchetti, V. Vitelli, Topological active matter, arXiv preprint arXiv:2010.00364 (2020).

[27] T. B. Saw, A. Doostmohammadi, V. Nier, L. Kocgozlu, S. Thampi, Y. Toyama, P. Marcq, C. T. Lim, J. M. Yeomans, B. Ladoux, Topological defects in epithelia govern cell death and extrusion, Nature 544 (7649) (2017) 212–216.

[28] K. Kawaguchi, R. Kageyama, M. Sano, Topological defects control collective dynamics in neural progenitor cell cultures, Nature 545 (7654) (2017) 327–331.

[29] T. Sanchez, D. T. Chen, S. J. DeCamp, M. Heymann, Z. Dogic, Spontaneous motion in hierarchically assembled active matter, Nature 491 (7424) (2012) 431–434.

[30] E. G. Virga, Variational Theories for Liquid Crystals, 1st Edition, Vol. 8, Chapman and Hall, London, 1994.

[31] J. M. Ball, A. Majumdar, Nematic liquid crystals: from maier-saupe to a continuum theory, Molecular crystals and liquid crystals 525 (1) (2010) 1–11.

[32] P. Bauman, D. Phillips, Regularity and the behavior of eigenvalues for minimizers of a constrained q-tensor energy for liquid crystals, Calculus of Variations and Partial Differential Equations 55 (4) (2016) 81.

[33] L. Longa, D. Monselesan, H.-R. Trebin, An extension of the landau-ginzburg-de gennes theory for liquid crystals, Liquid Crystals 2 (6) (1987) 769–796.

[34] G. Fredrickson, et al., The equilibrium theory of inhomogeneous polymers, Vol. 134, Oxford University Press on Demand, 2006.

[35] I. Bajc, F. Hecht, S. Žumer, A mesh adaptivity scheme on the landau-de gennes functional minimization case in 3d, and its driving efficiency, Journal of Computational Physics 321 (2016) 981 – 996. doi:https://doi.org/10.1016/j.jcp.2016.02.072.
URL http://www.sciencedirect.com/science/article/pii/S0021999116001443

[36] T. Davis, E. Gartland, Finite element analysis of the landau-de gennes minimization problem for liquid crystals, SIAM Journal on Numerical Analysis 35 (1) (1998) 336–362. arXiv:https://doi.org/10.1137/S0036142996297448, doi:10.1137/S0036142996297448.
URL https://doi.org/10.1137/S0036142996297448

[37] M. Ravnik, S. Žumer, Landau-degennes modelling of nematic liquid crystal colloids, Liquid Crystals 36 (10-11) (2009) 1201–1214. arXiv:https://doi.org/10.1080/02678290903056095, doi:10.1080/02678290903056095.
URL https://doi.org/10.1080/02678290903056095

[38] S. Bartels, A. Raisch, Simulation of q-tensor fields with constant orientational order parameter in the theory of uniaxial nematic liquid crystals, in: M. Griebel (Ed.), Singular Phenomena and Scaling in Mathematical Models, Springer International Publishing, 2014, pp. 383–412. doi:10.1007/978-3-319-00786-1_17.

[39] J.-P. Borthagaray, R. H. Nochetto, S. W. Walker, A structure-preserving FEM for the uniaxially constrained **Q**-tensor model of nematic liquid crystals, Numerische Mathematik 145 (2020) 837 – 881. doi:10.1007/s00211-020-01133-z.
URL https://doi.org/10.1007/s00211-020-01133-z

[40] G.-D. Lee, J. Anderson, P. J. Bos, Fast q-tensor method for modeling liquid crystal director configurations with defects, Applied Physics Letters 81 (21) (2002) 3951–3953. arXiv:https://doi.org/10.1063/1.1523157, doi:10.1063/1.1523157.
URL https://doi.org/10.1063/1.1523157

[41] J. Zhao, Q. Wang, Semi-discrete energy-stable schemes for a tensor-based hydrodynamic model of nematic liquid crystal flows, Journal of Scientific Computing 68 (3) (2016) 1241–1266. doi:10.1007/s10915-016-0177-x.
URL https://doi.org/10.1007/s10915-016-0177-x

[42] C. D. Schimming, J. Viñals, Computational molecular field theory for nematic liquid crystals, Physical Review E 101 (3) (2020) 032702.

[43] C. D. Schimming, J. Viñals, Anisotropic disclination cores in nematic liquid crystals modeled by a self-consistent molecular field theory, Physical Review E 102 (1) (2020) 010701(R).

[44] H. Mori, J. Eugene C. Gartland, J. R. Kelly, P. J. Bos, Multidimensional director modeling using the q tensor representation in a liquid crystal cell and its application to the pi-cell with patterned electrodes, Japanese Journal of Applied Physics 38 (1R) (1999) 135.
URL http://stacks.iop.org/1347-4065/38/i=1R/a=135

[45] N. J. Mottram, C. J. P. Newton, Introduction to Q-tensor theory, ArXiv e-prints (Sep. 2014). arXiv:1409.3542.

[46] J. Eugene C. Gartland, Scalings and limits of landau-de gennes models for liquid crystals: a comment on some recent analytical papers, Mathematical Modelling and Analysis 23 (3) (2018) 414 – 432. doi:https://doi.org/10.3846/mma.2018.025.

[47] A. M. Sonnet, E. Virga, Dissipative Ordered Fluids: Theories for Liquid Crystals, Springer, 2012.

[48] G. Barbero, G. Durand, On the validity of the rapini-papoular surface anchoring energy form in nematic liquid crystals, J. Phys. France 47 (12) (1986) 2129–2134. doi:10.1051/jphys:0198600470120212900.
URL https://doi.org/10.1051/jphys:0198600470120212900

[49] S. W. Walker, On The Correct Thermo-dynamic Potential for Electro-static Dielectric Energy, ArXiv e-prints (Mar. 2018). arXiv:1803.08136.

[50] R. P. Feynman, R. B. Leighton, M. Sands, The Feynman Lectures on Physics, Addison-Wesley Publishing Company, 1964.

[51] P. Biscari, P. Cesana, Ordering effects in electric splay freedericksz transitions, Continuum Mechanics and Thermodynamics 19 (5) (2007) 285–298. doi:10.1007/s00161-007-0055-8.

[52] A. Majumdar, Equilibrium order parameters of nematic liquid crystals in the landau-de gennes theory, European Journal of Applied Mathematics 21 (2) (2010) 181–203. doi:10.1017/S0956792509990210.

[53] J. Katriel, G. F. Kventsel, G. R. Luckhurst, T. J. Sluckin, Free energies in the landau and molecular field approaches, Liquid Crystals 1 (4) (1986) 337–355. arXiv:https://doi.org/10.1080/02678298608086667, doi:10.1080/02678298608086667.
URL https://doi.org/10.1080/02678298608086667

[54] E. C. Gartland Jr, P. Palffy-Muhoray, R. S. Varga, Numerical minimization of the Landau-de Gennes free energy: Defects in cylindrical capillaries, Molecular Crystals and Liquid Crystals 199 (1) (1991) 429–452.

[55] L. C. Evans, Partial Differential Equations, American Mathematical Society, Providence, Rhode Island, 1998.

[56] A. Braides, Gamma-Convergence for Beginners, Vol. 22 of Oxford Lecture Series in Mathematics and Its Applications, Oxford Scholarship, 2002.

[57] J. Jost, X. Li-Jost, Calculus of Variations, Cambridge, 1998.

[58] A. Friedman, Partial Differential Equations of Parabolic Type, Dover, 2008.

[59] N. V. Krylov, Lectures on Elliptic and Parabolic Equations in Sobolev Spaces, Graduate Studies in Mathematics, American Mathematical Society, 2008.

[60] G. D. Maso, M. Forti, M. Miranda, S. A. Spagnolo, L. Ambrosio (Eds.), Selected Papers, Springer Collected Works in Mathematics, Ennio De Giorgi, 2006.

[61] S. M. Wise, C. Wang, J. S. Lowengrub, An energy-stable and convergent finite-difference scheme for the phase field crystal equation, SIAM J. Numer. Anal. 47 (3) (2009) 2269–2288. doi:10.1137/080738143.

[62] J. Xu, Y. Li, S. Wu, A. Bousquet, On the stability and accuracy of partially and fully implicit schemes for phase field modeling, Computer Methods in Applied Mechanics and Engineering 345 (2019) 826 – 853. doi:https://doi.org/10.1016/j.cma.2018.09.017.
URL http://www.sciencedirect.com/science/article/pii/S0045782518304687

[63] V. I. Lebedev, D. N. Laikov, A quadrature formula for the sphere of the 131st algebraic order of accuracy, Doklady Mathematics 59 (3) (1999) 477 – 481.

[64] S. W. Walker, FELICITY: A Matlab/C++ toolbox for developing finite element methods and simulation modeling, SIAM Journal on Scientific Computing 40 (2) (2018) C234–C257. arXiv:https://doi.org/10.1137/17M1128745, doi:10.1137/17M1128745.
URL https://doi.org/10.1137/17M1128745

[65] S. W. Walker, FELICITY finite element toolbox, https://github.com/walkersw/felicity-finite-element-toolbox/ (2021).

[66] Y. Notay, An aggregation-based algebraic multigrid method, Electronic Transactions On Numerical Analysis 37 (2010) 123–146.

[67] A. Napov, Y. Notay, Algebraic analysis of aggregation-based multigrid, Numerical Linear Algebra with Applications 18 (3) (2011) 539–564. doi:10.1002/nla.741.

[68] A. Napov, Y. Notay, An algebraic multigrid method with guaranteed convergence rate, SIAM Journal on Scientific Computing 34 (2) (2012) A1079–A1109. arXiv:http://dx.doi.org/10.1137/100818509, doi:10.1137/100818509.

[69] Y. Notay, Aggregation-based algebraic multigrid for convection-diffusion equations, SIAM Journal on Scientific Computing 34 (4) (2012) A2288–A2316. arXiv:http://dx.doi.org/10.1137/110835347, doi:10.1137/110835347.

[70] S. Zhou, S. V. Shiyanovskii, H.-S. Park, O. D. Lavrentovich, Fine structure of the topological defect cores studied for disclinations in lyotropic chromonic liquid crystals, Nature Communications 8 (1) (2017) 14974. doi:10.1038/ncomms14974.
URL https://doi.org/10.1038/ncomms14974

[71] S. Alama, L. Bronsard, X. Lamy, Analytical description of the saturn-ring defect in nematic colloids, Phys. Rev. E 93 (2016) 012705. doi:10.1103/PhysRevE.93.012705.

[72] Y. Gu, N. L. Abbott, Observation of saturn-ring defects around solid microspheres in nematic liquid crystals, Phys. Rev. Lett. 85 (2000) 4719–4722. doi:10.1103/PhysRevLett.85.4719.